A mitochondrial carrier transports glycolytic intermediates to link cytosolic and mitochondrial glycolysis in the human gut parasite *Blastocystis*

Eva Pyrihová[1,2], Martin S. King[1], Alannah C. King[1], M. Rey Toleco[2], Mark van der Giezen[2]* and Edmund R.S. Kunji[1]*

[1]Medical Research Council Mitochondrial Biology Unit, The Keith Peters Building, Cambridge Biomedical Campus, Hills Road, Cambridge, CB2 0XY, United Kingdom.

[2]University of Stavanger, Department of Chemistry, Bioscience, and Environmental Engineering, Richard Johnsens gate 4, N-4021 Stavanger, Norway.

*Authors to whom correspondence should be addressed

Tel.: +47 5183 4493, e-mail: mark.vandergiezen@uis.no

Tel.: + 44 1223 252850, e-mail: ek@mrc-mbu.cam.ac.uk

Key words

Bioenergetics, SLC25 mitochondrial carrier family, missing transport link, carboxylate carriers, thermostability shift assays, transport assays, anaerobic and aerobic metabolism, protists, parasites.

Abstract

Stramenopiles form a clade of diverse eukaryotic organisms, including multicellular algae, the fish and plant pathogenic oomycetes, such as the potato blight *Phytophthora,* and the human intestinal protozoan *Blastocystis*. In most eukaryotes, glycolysis is a strictly cytosolic metabolic pathway that converts glucose to pyruvate, resulting in the production of NADH and ATP. In contrast, stramenopiles have a branched glycolysis in which the enzymes of the pay-off phase are located in both the cytosol and the mitochondrial matrix. Here, we identify a mitochondrial carrier in *Blastocystis* that can transport glycolytic intermediates, such as dihydroxyacetone phosphate and glyceraldehyde-3-phosphate, across the mitochondrial inner membrane, linking the cytosolic and mitochondrial branches of glycolysis. Comparative analyses with the phylogenetically-related human mitochondrial oxoglutarate carrier (SLC25A11) and dicarboxylate carrier (SLC25A10) show that the glycolytic intermediate carrier has lost its ability to transport the canonical substrates malate and oxoglutarate. *Blastocystis* lacks several key components of oxidative phosphorylation required for the generation of mitochondrial ATP, such as complexes III and IV, ATP synthase and ADP/ATP carriers. The presence of the glycolytic pay-off phase in the mitochondrial matrix generates ATP, which powers energy-requiring processes, such as macromolecular synthesis, as well as NADH, used by mitochondrial complex I to generate a proton motive force to drive the import of proteins and molecules. Given its unique substrate specificity and central role in carbon and energy metabolism, the carrier for glycolytic intermediates identified here represents a specific drug and pesticide target against stramenopile pathogens, which are of great economic importance.

Introduction

Glycolysis is a crucial metabolic pathway that most organisms use to obtain energy from the oxidation of sugars, which consists of ten enzymatic reactions in total, divided into two phases. The first 'preparatory' phase consists of five reactions, the products of which are the triose phosphates dihydroxyacetone phosphate and glyceraldehyde-3-phosphate. The second 'pay-off' phase leads to the production of ATP, NADH and pyruvate, which is transported into the mitochondrial matrix by the mitochondrial pyruvate carrier (Bricker et al., 2012; Herzig et al., 2012). In most eukaryotes, glycolysis is a cytosolic process with the exception of trypanosomes, where it is localised in the glycosomes (Opperdoes and Borst, 1977). However, it was recently discovered that a large group of eukaryotes, the stramenopiles, have a branched glycolytic pathway in which the pay-off phase is duplicated and also localised in mitochondria (Abrahamian et al., 2017; Bártulos et al., 2018). The stramenopiles are an extremely diverse eukaryotic group consisting mainly of protist algae, which are among the most important primary oxygen producers in the oceans (Burki et al., 2020). The group also includes multicellular algae (kelps) and the economically-devastating oomycetes, such as *Phytophthora infestans* (Jiang and Tyler, 2012), which causes potato blight, one of the major contributing factors of the Great Famine in Ireland in the late 19th century.

The human gut protozoan *Blastocystis* also belongs to the stramenopiles. Despite more than one billion infected individuals worldwide (Andersen and Stensvold, 2016), the public health significance of *Blastocystis* is debated. *Blastocystis* is often linked to patients with diarrhoea, irritable bowel syndrome (Poirier et al., 2012), or inflammatory bowel disease (Dogruman-Al et al., 2009). However, it is also frequently found in healthy individuals, and a few microbiome studies associated *Blastocystis* with higher microbial diversity (Andersen et al., 2015; Audebert et al., 2016; Stensvold et al., 2022). The controversy may arise from the extreme genetic diversity of *Blastocystis*, which is classified into over 40 subtypes (Andersen et al., 2015; Stensvold et al., 2023), and thus its influence on gut microbiota is likely to be subtype-specific (Tito et al., 2019). Nevertheless, *Blastocystis* ST7-B, which was used in this study, is most frequently associated with pathogenic phenotypes (Ajjampur et al., 2016; Deng et al., 2023; Stensvold et al., 2009; Wu et al., 2014; Yason et al., 2019) and was recently linked to a decreased microbial diversity in diarrheal patients (Deng et al., 2022). The treatment of choice is metronidazole (Stenzel and Boreham, 1996), but there have been reports of resistance

72 (Haresh et al., 1999; Mirza et al., 2011; Moghaddam et al., 2005), highlighting the need for new
73 therapeutic interventions.
74
75 Unlike other stramenopiles, *Blastocystis* has lost the cytosolic pay-off phase of glycolysis,
76 consistent with the absence of a gene encoding a mitochondrial pyruvate carrier (Bártulos et
77 al., 2018). The only exception is the last enzyme of the pathway, pyruvate kinase, which was
78 also identified as a cytosolic protein (Lantsman et al., 2008). *Blastocystis* is an anaerobe (Zierdt,
79 1991) with highly divergent mitochondria (Stechmann et al., 2008). It has respiratory
80 complexes I and II, but lacks the rest of the electron transport chain, as well as ATP synthase
81 and mitochondrial ADP/ATP carriers (Gentekaki et al., 2017; Stechmann et al., 2008;
82 Wawrzyniak et al., 2008). Therefore, *Blastocystis* relies mainly on glycolysis and fermentation
83 for its metabolic energy requirements (Müller et al., 2012). The transport of glycolytic
84 intermediates across the mitochondrial inner membrane is necessary for the completion of
85 glycolysis and is critical for the survival of the parasite. Glycolytic enzymes are powerful drug
86 targets in parasites that are strictly dependent on glycolysis for ATP production. The structural
87 differences between host and parasitic glyceraldehyde-3-phosphate dehydrogenase and
88 triosephosphate isomerase in *Plasmodium falciparum* have been studied with the aim of
89 inhibiting glycolysis (Bruno et al., 2014; Penna-Coutinho et al., 2011; Ravindra and Balaram,
90 2005). Similarly, inhibitors against phosphofructokinase in *Trypanosoma brucei* have a rapid
91 effect on the parasite viability without inhibiting the host enzyme (McNae et al., 2021).
92 Understanding the unique aspects of parasite metabolism is crucial for the discovery of new
93 drug targets.
94
95 It is clear that the branched stramenopile glycolysis needs to be linked by a specific transporter
96 in the mitochondrial inner membrane, as the solute exchange between the cytosol and
97 mitochondrial matrix is tightly controlled (Kunji et al., 2020; Ruprecht and Kunji, 2020). The
98 mitochondrial carrier family (SLC25) is the largest solute transporter family in humans (Kunji et
99 al., 2020). Its members facilitate the transport of nucleotides, amino acids, inorganic ions, keto
100 acids, vitamins and other nutrients across the mitochondrial inner membrane. All SLC25
101 members have a three-fold pseudo-symmetric structure, evident at the sequence level by the
102 presence of three conserved homologous repeats (Saraste and Walker, 1982) and specific

103 motifs important for their transport mechanism (Ruprecht et al., 2019; Ruprecht and Kunji,
104 2020, 2021).
105
106 Here, we report a stramenopile-specific group of transport proteins closely related to
107 mitochondrial carboxylate carriers of the SLC25 family. We characterised one of these unique
108 *Blastocystis* carriers, which has lost its ability to transport the canonical substrates malate and
109 oxoglutarate. Instead, this carrier can transport several glycolytic intermediates, including
110 dihydroxyacetone phosphate, glyceraldehyde-3-phosphate, 3-phosphoglycerate and
111 phosphoenolpyruvate, thus providing a previously undiscovered transport link between
112 cytosolic and mitochondrial glycolysis. Since *Blastocystis* relies solely on mitochondrial
113 glycolysis, the inhibition of this carrier might represent a promising way to treat this parasite.
114

115 ## Results

116 ### A group of mitochondrial carboxylate carriers that is unique to stramenopiles

117 The last enzyme of the cytosolic phase of glycolysis in *Blastocystis* is triosephosphate isomerase
118 (Bártulos et al., 2018). Consequently, dihydroxyacetone phosphate and glyceraldehyde-3-
119 phosphate need to be transported into the mitochondrial matrix for the pay-off phase of
120 glycolysis. Given the presence of mitochondrial glycolysis in stramenopiles, we searched for a
121 transporter that is not only ubiquitous in stramenopiles, but also absent in other eukaryotes.
122 As glycolysis in *Blastocystis* would be critically dependent on this transporter, we used this
123 parasite as a model organism. We focused on mitochondrial carboxylate carriers because of
124 their ability to transport phosphorylated three-carbon substrates (Castegna et al., 2010;
125 Fiermonte et al., 2001; Palmieri et al., 1972) and compared the sequences of carboxylate
126 carriers from all major eukaryotic supergroups. Our analyses revealed four well-defined groups
127 of carriers: dicarboxylate carriers (DIC, SLC25A10), oxoglutarate/malate carriers (OGC,
128 SLC25A11), di/tricarboxylate carriers (DTC), and a new stramenopile-specific group, the
129 putative glycolytic intermediate carriers (GIC) (**Figure 1**). At least one copy of the putative GIC
130 carrier was identified in each stramenopile species. In *Blastocystis* ST7-B, there are four copies
131 of the putative GIC protein, but two of them are truncated and lack crucial mitochondrial carrier
132 elements (Ruprecht et al., 2019; Ruprecht and Kunji, 2020, 2021), possibly rendering these
133 proteins non-functional (XP_012899519.1 has an N-terminal truncation; XP_012896318.1 has
134 a C-terminal truncation) (Ruprecht and Kunji, 2020).

135

136 The unidentified *Blastocystis* carriers localise to mitochondria

137 Another important criterion is that the putative glycolytic intermediate carriers localise to
138 mitochondria in *Blastocystis*. Specific (peptide) rabbit antibodies were raised against the two
139 putative glycolytic intermediate carriers bGIC-1 and bGIC-2 as well as an ortholog of the
140 *Blastocystis* oxoglutarate carrier bOGC (**Figure 2B**). Mitochondria were visualized using
141 antibodies raised against a triosephosphate isomerase/glyceraldehyde-3-phosphate
142 dehydrogenase mitochondrial fusion protein (TPI-GAPDH) (Bártulos et al., 2018).
143 Immunoconfocal microscopy clearly show that bOGC, bGIC-1 and bGIC-2 localise to
144 mitochondria in *Blastocystis*, showing that they are potential candidates for the missing
145 transport links (**Figure 2A**).

146

147 Human and *Blastocystis* carriers purified from yeast mitochondria are folded

148 All three *Blastocystis* proteins were expressed in and purified from *Saccharomyces cerevisiae*
149 mitochondria using the detergent lauryl maltose neopentyl glycol (**Figure 3A**). They were
150 compared to the human oxoglutarate carrier SLC25A11 (hOGC) and dicarboxylate carrier
151 SLC25A10 (hDIC), prepared in the same way. Next, thermostability analysis was used to assess
152 whether the purified proteins are correctly folded. Spectral properties of tryptophan/tyrosine
153 residues change as their local environment changes during protein denaturation in a
154 temperature ramp (Alexander et al., 2014). The assay produces an apparent melting
155 temperature (Tm) at which the rate of protein unfolding is the highest. All three proteins
156 produced unfolding curves, showing that they are folded. The apparent melting temperatures
157 for bOGC (52.6 ± 0.5 °C), bGIC-1 (60.7 ± 0.4 °C) and bGIC-2 (59.8 ± 0.4 °C) (**Figure 3B** and **C**) are
158 similar to those observed for hOGC (51.0 °C), hDIC (54.1 °C) and other mitochondrial carriers
159 (Crichton et al., 2015; Jaiquel Baron et al., 2021; Majd et al., 2018).

160

161 Two mitochondrial carriers of *Blastocystis* bind glycolytic intermediates

162 We have previously shown that inhibitors (Crichton et al., 2015; Jaiquel Baron et al., 2021;
163 Tavoulari et al., 2022) and substrates (Majd et al., 2018; Mavridou et al., 2022) can specifically
164 stabilize a population of transport proteins in thermal denaturation assays. This technique
165 provides a simple, high-throughput method for screening libraries of compounds to identify
166 potential protein binders that can then be confirmed in low-throughput transport assays with

167 radiolabelled substrates (Majd et al., 2018). We used detergent-solubilized, purified protein to
168 screen a library of 39 commercially available compounds, which included mono-, di- and
169 tricarboxylates, acids, inorganic ions, and several glycolytic intermediates (with the exception
170 of 1,3-bisphosphoglycerate and 2-phosphoglycerate, which were not available).
171
172 In order to quantify the binding effect of a compound, we calculated a thermostability shift
173 (ΔTm) by subtracting the apparent melting temperature in the absence of a compound from
174 that in its presence. A positive shift suggests that the compound is stabilizing, indicating a
175 putative substrate (Majd et al., 2018). We first tested the library on purified hOGC (SLC25A11)
176 and hDIC (SLC25A10). A range of compounds had stabilizing effects on hOGC in thermostability
177 shift assays (**Figure 4A**). Oxoglutarate (3.8 ± 0.4 °C), malate (3.6 ± 0.3 °C), maleate (3.1 ± 0.1
178 °C), succinate (1.9 ± 0.3 °C) and malonate (1.3 ± 0.2 °C) all produced positive shifts. For hDIC,
179 larger shifts than for hOGC were observed for malate (4.8 ± 0.2 °C), maleate (8.0 ± 0.1 °C),
180 succinate (3.0 ± 0.3 °C) and malonate (7.3 ± 0.1 °C) (**Figure 4B**). Shifts were also observed for
181 sulphate (3.0 ± 0.2 °C), thiosulphate (4.0 ± 0.4 °C), phosphate (3.2 ± 0.2 °C), dihydroxyacetone
182 phosphate (2.5 ± 0.4 °C) and glyceraldehyde-3-phosphate (5.6 ± 0.6 °C) (**Figure 4B**), which were
183 not observed for hOGC and may reflect a difference in substrate specificity (Crompton et al.,
184 1974).
185
186 The thermostability shifts for the *Blastocystis* ortholog bOGC were similar to those of hOGC
187 (SLC25A11), although some compounds, most notably citrate and isocitrate, produced small
188 stabilizations that were not observed for the human ortholog (**Figure 4C**). A wider range of
189 compounds caused an increase in stability of the two candidate carriers bGIC-1 and bGIC-2
190 compared to bOGC (**Figure 4D** and **E**). These compounds included glycolytic intermediates,
191 such as glyceraldehyde-3-phosphate (1.0 ± 0.1 °C and 2.1 ± 0.1 °C for bGIC-1 and bGIC-2,
192 respectively) and dihydroxyacetone phosphate (3.6 ± 0.2 °C and 1.6 ± 0.1 °C) and inorganic
193 ions, such as phosphate (1.7 ± 0.1 °C and 5.0 ± 0.1 °C) and sulphate (2.3 ± 0.2 °C and 2.6 ± 0.3
194 °C). A significant shift was observed for phosphoenolpyruvate (PEP) in the case of bGIC-2 (4.3
195 ± 0.2 °C). In comparison, hOGC showed no shift for any of these compounds (**Figure 4A**),
196 whereas bOGC showed only a minor shift in the presence of sulphate (0.5 ± 0.1 °C) (**Figure 4C**).
197

198 *Blastocystis* GIC-2 is a functional mitochondrial carrier

199 We first tested [^{14}C]-malate/malate homo-exchange for bGIC-1 and bGIC-2 (**Figure 5A** and **B**,
200 respectively). No transport was measured, showing that these proteins do not have the ability
201 to transport malate. We next aimed to find a radiolabelled substrate that is transported by
202 bGIC-1 and bGIC-2. We tested [^{33}P]-phosphate/phosphate and [^{35}S]-sulphate/sulphate homo-
203 exchange, as both compounds induce relatively large shifts in thermostability assays: bGIC-1
204 (1.7 ± 0.1 °C and 2.3 ± 0.2 °C) and bGIC-2 (5.0 ± 0.1 °C and 2.6 ± 0.3 °C), for phosphate and
205 sulphate, respectively (**Figure 4D** and **E**). No transport was detected for either phosphate
206 (**Figure 5C**) or sulphate (**Figure 5E**) for bGIC-1. In contrast, bGIC-2 showed transport activity for
207 both: the rate of [^{33}P]-phosphate/phosphate homo-exchange was 4.5 times above the
208 background (**Figure 5D**), and the rate of [^{35}S]-sulphate/sulphate homo-exchange was 22 times
209 above background (**Figure 5F**). These data show that bGIC-2 is a functional mitochondrial
210 carrier.

211

212 Human OGC and DIC have distinct and overlapping substrate specificities

213 In addition to the glycolytic intermediates that were the focus of this study, we selected all
214 compounds that stabilized the proteins in thermostability assays and performed transport
215 assays. To test whether a compound was transported, we loaded proteoliposomes with
216 substrate by freeze-thaw-extrusion (Jaiquel Baron et al., 2021), and initiated exchange with the
217 addition of radiolabelled [^{14}C]-malate (hOGC and bOGC, **Figure 3D** and **E**) or [^{35}S]-sulphate
218 (hDIC). Only when the internalized compound is a transported substrate of the carrier will the
219 uptake of radiolabelled substrate occur. For hOGC (SLC25A11), uptake was measured for
220 oxoglutarate, oxaloacetate, malate, succinate, maleate, malonate, 2-oxoadipate (**Figure 6A**).
221 Surprisingly, a low uptake rate was measured for pyruvate, which did not induce a significant
222 shift (0.1 ± 0.3 °C). Pyruvate is a small molecule and therefore probably does not introduce
223 enough additional bonds to stabilize the protein. The substrate specificity of hOGC is similar to
224 that of the rat and bovine oxoglutarate carrier (Bisaccia et al., 1988; Fiermonte et al., 1993;
225 Palmieri et al., 1972). For hDIC (SLC25A10), uptake was observed for malate, succinate,
226 maleate, malonate, sulphate, thiosulphate, phosphate and, to a lesser extent, oxalic acid and
227 dihydroxyacetone phosphate (**Figure 6B**). This result is consistent with previous data that have
228 shown that the rat dicarboxylate carrier also transports sulphate and thiosulphate in addition
229 to dicarboxylates (Crompton et al., 1974; Saris, 1980). Although we measured transport for

230 dihydroxyacetone phosphate, we have not found any evidence for the presence of
231 dihydroxyacetone phosphate inside mitochondria in the literature. It is possible that it is not
232 transported under physiological conditions in competition with dicarboxylates or other
233 substrates. The substrate specificity of *Blastocystis* OGC (**Figure 6C**) is very similar to human
234 OGC (**Figure 6A**), consistent with their close phylogenetic relationship.
235
236 ***Blastocystis* GIC-2 links cytosolic and mitochondrial glycolysis**
237 We used [^{35}S]-sulphate as a counter-substrate and tested hetero-exchange to determine the
238 substrate specificity of bGIC-2 (**Figure 6D**). No transport was observed for the canonical
239 oxoglutarate carrier substrates, including oxaloacetate, malate, succinate and 2-oxoadipate;
240 oxoglutarate, maleate and malonate displayed only low transport rates. Interestingly, bGIC-2
241 displayed high transport rates for phosphate, sulphate, and thiosulphate and for the glycolytic
242 intermediates dihydroxyacetone phosphate, glyceraldehyde-3-phosphate, 3-phosphoglycerate
243 and phosphoenolpyruvate (**Figure 6D**).
244
245 **Discussion**
246 Glycolysis is a textbook example of a well-conserved cytosolic pathway. However, the discovery
247 that glycolysis is branched and also mitochondrial in stramenopiles (Abrahamian et al., 2017;
248 Bártulos et al., 2018; Nakayama et al., 2012) raises questions about how glycolytic
249 intermediates are transported across the tightly controlled mitochondrial inner membrane.
250 Here, we report the discovery and characterisation of a mitochondrial carrier protein unique
251 to stramenopiles that transports the glycolytic intermediates dihydroxyacetone phosphate,
252 glyceraldehyde-3-phosphate and phosphoenolpyruvate, providing the heretofore missing
253 transport link.
254
255 Since mitochondrial glycolysis is found exclusively in stramenopiles, we searched for a
256 transporter that is ubiquitous in these species, but not in other eukaryotes. Phylogenetic
257 analyses identified a new class of mitochondrial carboxylate carriers in stramenopiles that are
258 most closely related to plant di/tricarboxylate carriers (**Figure 1**). The plant carriers catalyse the
259 transport of tricarboxylates (citrate, isocitrate, and aconitate) in exchange for dicarboxylates
260 (oxoglutarate, oxaloacetate, malate, maleate, succinate, and malonate) (Picault et al., 2002)
261 and are also present in Alveolata, Rhizaria, and Haptophyta (Toleco et al., 2020), which share a

262 common evolutionary ancestor with stramenopiles (Burki et al., 2020). Therefore, the glycolytic
263 intermediate carrier of stramenopiles is probably derived from a common ancestor with
264 di/tricarboxylate carriers and does not exist in any other eukaryote outside of the stramenopile
265 clade.
266
267 *Blastocystis* was used in this study as a stramenopile model organism, as it relies solely on
268 glycolysis for its energy demands and does not have a second branch of glycolysis in the cytosol.
269 We characterised human and *Blastocystis* carboxylate carriers and demonstrated that the
270 stramenopile GIC proteins have a unique substrate specificity that is distinct from the human
271 carriers (**Figure 6**). We also characterised the substrate specificity of *Blastocystis* OGC, which
272 has the same specificity as human OGC (SLC25A11), and we demonstrated that it is unable to
273 transport glycolytic intermediates and thus could not be the missing transport step in the
274 branched glycolytic pathway.
275
276 *Blastocystis* GIC-1 did not transport any of the tested substrates (**Figure 5A**, **C** and **E**), but it is
277 expressed and localised to mitochondria (**Figure 2A**), demonstrating that it is not a
278 pseudogene. We did not test radiolabelled glycolytic intermediates directly in transport, as
279 phosphoenolpyruvate and dihydroxyacetone phosphate are not available, and radiolabelled
280 glyceraldehyde-3-phosphate is prohibitively expensive. We cannot, therefore, exclude the
281 possibility that GIC-1 catalyses glycolytic intermediate exchange, but not in hetero-exchange
282 reactions with malate, phosphate and sulphate. It is more likely that bGIC-1 has lost its
283 transport activity and could possibly fulfil a different role. For example, in *Tetrahymena*
284 *thermophila*, a non-functional OGC-like carrier is incorporated into a respiratory supercomplex
285 (Zhou et al., 2022). In contrast to bGIC-1, bGIC-2 transports several inorganic ions and glycolytic
286 intermediates, including dihydroxyacetone phosphate and glyceraldehyde-3-phosphate
287 (**Figure 6D**), but not the canonical substrates of *Blastocystis* OGC, such as malate, maleate,
288 malonate, and succinate. Most mitochondrial carriers operate as strict antiporters, where the
289 chemical gradient of one substrate drives the uptake of the counter-substrate (Ruprecht and
290 Kunji, 2020). A mitochondrial phosphate carrier homolog was identified in the phylogenetic
291 analysis of *Blastocystis* (**Figure 1 - figure supplement 1**), which is driven by the proton motive
292 force to maintain high concentrations of phosphate in the mitochondrial matrix, which in turn
293 could drive the uptake of glycolytic intermediates. *Blastocystis* lacks many of the conserved

294 carrier proteins found in the mitochondria of aerobes. In total, we have only identified 18
295 mitochondrial carriers in *Blastocystis* (**Figure 1 - figure supplement 1**). However, we show that
296 bGIC-2 seems to be able to compensate for the loss of some mitochondrial carriers, including
297 the transport of inorganic ions in the absence of a DIC homolog. Additionally, the distantly
298 related citrate carrier, which transports dicarboxylates, tricarboxylates and PEP, was also lost
299 in *Blastocystis*, possibly due to an incomplete TCA cycle devoid of citrate synthase, aconitase,
300 isocitrate dehydrogenase and α-ketoglutarate dehydrogenase (Stechmann et al., 2008; Zierdt
301 et al., 1988). In *Blastocystis*, PEP can be synthesised from mitochondrial pyruvate via
302 oxaloacetate (Gentekaki et al., 2017; Stechmann et al., 2008), and here we show that PEP
303 transport is catalysed by bGIC-2. When PEP is exported by bGIC-2, it could be converted into
304 pyruvate and lactate by cytosolic pyruvate kinase and lactate dehydrogenase, respectively
305 (Lantsman et al., 2008), which would lead to the synthesis of ATP and the conversion of NADH
306 to NAD^+ in the cytosol. This reaction may play a significant role in cytosolic ATP generation, as
307 there is no mitochondrial ADP/ATP carrier in *Blastocystis* for adenine nucleotide exchange
308 (**Figure 1 - figure supplement 1**). *Blastocystis* also contains a glycerol-3-phosphate
309 dehydrogenase (Gentekaki et al., 2017), which oxidises NADH to convert glycerol-3-phosphate
310 to dihydroxyacetone phosphate, which in turn can be transported into mitochondria by bGIC-
311 2 to generate ATP and reducing equivalents. In most other eukaryotes, cytosolic NADH is
312 oxidised by the malate-aspartate shuttle, but this pathway requires an ortholog of the
313 mitochondrial aspartate/glutamate carrier, which could not be identified in *Blastocystis*, even
314 though it might have a mitochondrial glutamate carrier (**Figure 1 - figure supplement 1**).
315
316 What selective advantage could there be to have the pay-off phase of glycolysis in the
317 mitochondrial matrix? *Blastocystis* is well adapted to an anoxic environment with its anaerobic
318 metabolism but has a limited ability to detoxify oxygen. In its natural environment, *Blastocystis*
319 likely uses protons as terminal electron acceptors by using pyruvate:ferredoxin oxidoreductase,
320 which would result in the production of hydrogen and a range of fermentative products, such
321 as lactate, acetate, and propionate (Gentekaki et al., 2017; Lantsman et al., 2008; Stechmann
322 et al., 2008). Under aerobic stress, such as in a dysbiotic gut (Stensvold and van der Giezen,
323 2018), it possibly uses oxygen as the terminal electron acceptor by using alternative oxidase,
324 which produces water (Tsaousis et al., 2018). However, as a likely adaptation to the anoxic
325 environment, *Blastocystis* has lost some of the canonical components of oxidative

326 phosphorylation, including complexes III and IV of the respiratory chain, ATP-synthase and
327 mitochondrial ADP/ATP carriers (Stechmann et al., 2008). Consequently, it has lost its ability to
328 synthesize mitochondrial ATP via this route. This role was taken over by transfer of the pay-off
329 phase of glycolysis to the mitochondrial matrix in *Blastocystis*, which has several advantages.
330 The degradation of one glucose molecule in the cytosol requires one ATP and one
331 pyrophosphate molecule, but will generate four ATP molecules in the mitochondrial matrix,
332 which can be used for ATP-requiring processes, such as protein import, mitochondrial DNA
333 replication and transcription, and mitochondrial protein synthesis (Denoeud et al., 2011;
334 Gentekaki et al., 2017). In addition, two NAD^+ molecules are reduced to NADH, which can be
335 used by complex I to generate a proton motive force to drive the import of proteins and the
336 uptake of ions and molecules into mitochondria, such as phosphate. Cytosolic ATP can be
337 supplied either through the export of PEP by bGIC-2, as explained, or via a mitochondrial carrier
338 that shares properties with the mitochondrial Mg-ATP/Pi carrier, which is generally used to
339 equilibrate adenine nucleotide pools between the matrix and cytosol.
340
341 Our results show that the canonical metabolic pathways studied in common model organisms
342 can be altered in non-model eukaryotic species (**Figure 7**). Moreover, the newly discovered
343 glycolytic intermediates carrier demonstrates the plasticity of mitochondrial carriers in terms
344 of their substrate specificity. Through the discovery of this carrier, we have linked the two
345 halves of glycolysis and provided a potential target for specific treatment not only for
346 *Blastocystis* but also for other stramenopile pathogens that threaten global food security.
347
348 ## Materials and Methods
349 ### *In-silico* analysis
350 Bioinformatics-based approaches were used to identify potential candidates for a glycolytic
351 intermediate transporter. Any potential transporter should be present in all stramenopiles, but
352 absent in other eukaryotes, and could plausibly transport phosphorylated three carbon
353 substrates. Most of the transport proteins in mitochondria belong to the mitochondrial carrier
354 family (SLC25) (Kunji et al., 2020; Ruprecht and Kunji, 2020), and thus the initial search focused
355 on them.
356

357 Mitochondrial carrier sequences were gathered using 53 human mitochondrial carriers as a
358 BLAST query against the genomes of selected stramenopiles: *Blastocystis* ST7-B*, Aureococcus*
359 *anophagefferens, Ectocarpus sp.*, *Saprolegnia parasitica, Phaeodactylum tricornutum* and
360 *Phytopthora infestans*. InterProScan (www.ebi.ac.uk/interpro/search/sequence/) was then
361 used to discard non-carrier hits (Jones et al., 2014), and partial sequences were removed
362 (sequences with fewer than three signature repeats or 250 amino acids). Reciprocal BLAST was
363 then used to eliminate incorrectly assigned sequences. The stramenopile sequences were
364 aligned to *Homo sapiens, Saccharomyces cerevisiae* and *Arabidopsis thaliana* carriers. To
365 prepare the alignment for phylogenetic analysis, the structures of the ADP/ATP carrier (PDB:
366 1OKC and 6GCI) were used to identify and remove the hypervariable loop regions in each
367 sequence.
368
369 IQ-TREE was used to calculate a phylogenetic tree using an LG + F + R9 model suggested by
370 ModelFinder and branch supports were generated by ultrafast bootstrap with 1000 replicates
371 (Hoang et al., 2018; Minh et al., 2020). A clade of stramenopile-specific transporters was
372 identified as a sister group to the *A. thaliana* di/tricarboxylate carrier homologs (DTC) (**Figure**
373 **1 - figure supplement 1**). Within this clade, all selected stramenopile species were represented
374 at least once. Interestingly, *Blastocystis,* which has no homolog of the mitochondrial pyruvate
375 carrier, and would have to rely solely on the import of glycolytic intermediates, has four copies
376 of this carrier. Given that DTC substrates are three-carbon dicarboxylates and tricarboxylates,
377 it is possible that a closely related carrier could transport phosphorylated three-carbon
378 substrates.
379
380 To investigate whether this clade is not only present in stramenopiles, but also unique to them,
381 BLAST searches were performed using the unique stramenopile sequences against genomes
382 from an expanded range of eukaryotes using NCBI and EukProt databases (Priyam et al., 2019).
383 The collected sequences were screened to remove partial and duplicate sequences and
384 sequences that shared contact points with carboxylate carriers (Kunji and Robinson, 2006;
385 Robinson and Kunji, 2006) were selected. They were added to a multiple sequence alignment
386 of the identified stramenopile carriers and other closely related transporters from the first tree.
387 The maximum likelihood tree was generated by IQ-TREE with the LG + F + R7 model suggested

388 by ModelFinder (Minh et al., 2020). Branch supports were generated by ultrafast bootstrap
389 with 1000 replicates (Hoang et al., 2018).
390
391 To address the absence of GIC in other species and exclude the possibility of its presence
392 outside of stramenopiles, we performed additional analyses. The stramenopile GIC sequences
393 were blasted against NCBI datasets encompassing major eukaryotic groups, and the top hits
394 were selected and aligned with GIC sequences. Phylogenetic analysis of this expanded dataset
395 revealed that the non-stramenopile carriers are more closely related to other carboxylate
396 carriers, indicating that even the carriers most similar to GIC do not fall within the GIC clade.
397 These analyses confirmed that the putative GIC carriers are universal in stramenopiles and also
398 unique to them.
399
400 Protein production in mitochondria of *Saccharomyces cerevisiae*
401 Genes (SLC25A11, the human oxoglutarate carrier (hOGC), UniProt accession code: Q02978;
402 SLC25A10, the human dicarboxylate carrier (hDIC), UniProt accession code: Q9UBX3;
403 *Blastocystis* ST7-B oxoglutarate carrier (bOGC) UniProt accession code: D8M7L1; *Blastocystis*
404 ST7-B potential glycolytic intermediate carrier 1 (bGIC-1), UniProt accession code: D8LYZ6;
405 *Blastocystis* ST7-B potential glycolytic intermediate carrier 2 (bGIC-2), UniProt accession code:
406 D8LWW2) were codon-optimized with N-terminal eight histidine tag and a Xa protease
407 cleavage site to aid purification (hOGC, Δ2-13; hDIC, GKP added (positions 2-4); bGIC-1, Δ2-3;
408 bGIC-2, Δ2). The modified genes were cloned into a pYES2/CT vector (Invitrogen) under the
409 control of an inducible galactose promoter, as previously described (King and Kunji, 2020), and
410 expressed in *Saccharomyces cerevisiae* (GenScript) strain W303.1B (hOGC and bGIC-2) or the
411 protease-deficient strain BJ2186 (hDIC, bOGC and bGIC-1). Transformants were selected on Sc-
412 Ura + 2 % (w/v) glucose plates. For large-scale expression, a pre-culture of cells grown in Sc-Ura
413 + 2% (w/v) glucose was inoculated into 50 L of YPG plus 0.1% glucose medium in an Applikon
414 Pilot Plant 140 L bioreactor. Cells were grown at 30 °C for 20 hours, induced with a final
415 concentration of either 0.4% (hOGC, hDIC and bGIC-1) or 2.0% (bOGC and bGIC-2) galactose,
416 grown for a further 4 (hOGC) or 8 hours (hDIC, bOGC, bGIC-1 and bGIC-2), and harvested by
417 centrifugation (4,000 *g*, 20 minutes, 4 °C). Alternatively, 15 L of culture were grown in shaker
418 flasks and induced as above. Crude mitochondria were prepared using a bead mill (Dyno-Mill
419 Multilab, Willy A. Bachofen AG) by established methods (King and Kunji, 2020).

420

421 Preparation of lipid for protein purification

422 Tetraoleoyl cardiolipin (18:1) powder was purchased from Avanti Polar Lipids. Lipids were
423 solubilized in 10% (w/v) lauryl maltose neopentyl glycol (Anatrace) by vortexing for 4 hours at
424 room temperature to give 10 mg mL^{-1} lipid in a 10% (w/v) detergent stock. The stocks were
425 stored in liquid nitrogen.

426

427 Protein purification by nickel affinity chromatography

428 Protein was purified as described previously for the human mitochondrial ADP/ATP carrier
429 (Jaiquel Baron et al., 2021). In total, 0.5 g of mitochondria were solubilized in 1.5% (w/v) lauryl
430 maltose neopentyl glycol, protease inhibitor tablet (Roche), 20 mM imidazole, and 150 mM
431 NaCl for one hour by rotation at 4 °C. The insoluble material was separated from the soluble
432 fraction by centrifugation (200,000 *g*, 45 minutes, 4 °C). Nickel Sepharose slurry (0.5 mL resin;
433 GE healthcare) was added to the soluble fraction; the mixture was stirred at 4 °C for one hour.
434 The nickel resin was harvested by centrifugation (100 *g*, 10 minutes, 4 °C), transferred to a
435 Proteus 1-step batch midi spin column (Generon), and washed with 40 column volumes of
436 buffer A (20 mM HEPES pH 7.0, 150 mM NaCl, 40 mM imidazole, 0.1 mg mL^{-1} tetraoleoyl
437 cardiolipin / 0.1% (w/v) lauryl maltose neopentyl glycol) (100 *g*, 5 minutes, 4 °C); followed by
438 10 column volumes of buffer B (20 mM HEPES pH 7.0, 50 mM NaCl, 0.1 mg mL^{-1} tetraoleoyl
439 cardiolipin / 0.1% (w/v) lauryl maltose neopentyl glycol) (100 *g*, 5 minutes, 4 °C). The nickel
440 resin was resuspended in buffer B and incubated with 10 mM imidazole, 20 µg factor Xa
441 protease (NEB) and 5 mM $CaCl_2$ with inversion at 10 °C overnight. Protein was eluted by
442 centrifugation on a spin column (100 *g*, 2 minutes, 4 °C). Imidazole and NaCl were removed
443 using a PD-10 desalting column according to the manufacturer's instructions (GE Healthcare)
444 at 4 °C and the concentration was determined by spectrometry (NanoDrop Technologies) at
445 280 nm using calculated extinction coefficients (hOGC: 29,000 M^{-1} cm^{-1}; hDIC: 20,900 M^{-1} cm^{-}
446 ^{1}; bOGC: 50,350 M^{-1} cm^{-1}; bGIC-1: 48,735 M^{-1} cm^{-1}; bGIC-2: 41,620 M^{-1} cm^{-1}).

447

448 Generation and testing of antibodies

449 Specific peptides (C+LSGEGTSEKLYSSSF for bOGC, C+IVAPGEARLGSIKMA for bGIC-1 and
450 C+TAAEGRISGMAIAKS for bGIC-2) were generated as a N-terminal Keyhole limpet haemocyanin
451 fusion to raise the antibodies in rabbits (Eurogentec). For Western blots, an overnight

452 incubation with 1:2,000 α-bOGC, 1:6,000 α-bGIC1, and 1:1,000 α-bGIC2 and one hour
453 incubation with secondary 1:20,000 goat α-rabbit-HRP (Millipore) against 100 ng of purified
454 protein was used. The membranes were developed with ECL Western Blotting Detection
455 Reagents (Amersham).
456
457 Cell culture
458 Axenic cultures of *Blastocystis* ST7-B were a generous gift from Professor Kevin S. W. Tan
459 (National University of Singapore) and were grown as described previously (Leonardi et al.,
460 2021).
461
462 Confocal microscopy
463 *Blastocystis* ST7-B cells were harvested by centrifugation (1,000 *g*, 10 minutes) at ambient
464 temperature. Cells were washed with pre-reduced PBS, and fixed with 4% methanol-free
465 formaldehyde (Thermo Fisher Scientific), incubated at 37 °C for 30 minutes. Fixed parasites
466 were permeabilized with 0.1% Triton X-100, and blocked with 3% BSA prior to antibody staining.
467 Rabbit antibodies against bGIC-1 , bGIC-2 , and bOGC (Eurogentec) were diluted with 3% BSA
468 in PBS with 0.01% Triton X-100 at 1:5000, 1:1000, and 1:1500, respectively, and incubated
469 overnight at 4 °C. Guinea pig anti-TPI-GAPDH (1:1000; Eurogentec), previously shown to localise
470 in the mitochondria (Bártulos et al., 2018) was used as an mitochondrial marker. Alexa Fluor™
471 488 conjugated goat anti-rabbit (A-21428, Invitrogen) and Alexa Fluor™ 555 conjugated goat
472 anti-guinea pig (A-11073, Invitrogen), used as secondary antibodies, were diluted with 3% BSA
473 in PBS with 0.01% Triton X-100 at 0.5 µg mL^{-1} and 2 µg mL^{-1}, respectively. Hoechst 33342 (5 µg
474 mL^{-1}, Thermo Fisher Scientific) was used to stain DNA. All immunofluorescence assays were
475 carried out in No. 1.5 high precision glass cover slips (Marienfeld) coated with 20 µg Cell-Tak
476 (Corning). Cells were mounted using ProLong™ Gold Antifade Mountant (Molecular Probes)
477 and cured overnight. Images were taken using a Leica SP8 laser scanning confocal microscope
478 (Leica Microsystems) equipped with oil immersion objective lens (Leica Microsystems, HC PL
479 APO CS2 100x/1.40 NA). Z-stacks were collected with a system-optimized sampling compliant
480 to the Nyquest-Shannon sampling theorem and with LAS X LIGHTNING deconvolution-
481 optimized settings (Leica Microsystems). Optical sections from the image stacks were further
482 processed using Fiji Version 1.54d.
483

484 Thermostability analysis

485 Thermal unfolding analyses were performed with dye-free differential scanning fluorimetry
486 (nanoDSF), which monitors the changes in the spectral properties of tryptophan and tyrosine
487 residues due to changes in their environment caused by unfolding (Alexander et al., 2014). The
488 proteins have the following number of tryptophans: hOGC (two); hDIC (one); bOGC (five); bGIC-
489 1 (five); bGIC-2 (four). Approximately 0.6 µg of protein and 10 mM substrate were added into
490 a final volume of 10 µL purification buffer B, and the samples were loaded into nanoDSF-grade
491 standard glass capillaries. The temperature was increased by 4 °C every minute from 25 to 95
492 °C, the intrinsic fluorescence was measured in a Prometheus NT.48 nanoDSF device, and the
493 apparent melting temperature (Tm) was calculated with the PR.ThermControl software
494 (NanoTemper Technologies).

495

496 Reconstitution of carrier protein into liposomes

497 A mix containing *Escherichia coli* polar lipid extract (Avanti Polar Lipids order number:
498 100600C), egg L-α-phosphatidylcholine (Avanti Polar Lipids order number: 840051C) and
499 tetraoleoyl cardiolipin (Avanti Polar Lipids order number: 710335C) in a 15:5:1 (w/w) ratio was
500 dried under a stream of nitrogen: 6.3 mg of total lipids were used per sample (0.625 mL). Lipids
501 were re-hydrated in 20 mM HEPES pH 7.0, 50 mM NaCl and 5 mM $MgCl_2$. The detergent
502 pentaethylene glycol monodecyl ether ($C_{10}E_5$) was added to a final concentration of 2.5% (v/v),
503 and the lipids were solubilized by vortexing and incubated on ice: the equivalent 30 µg protein
504 was added per sample. The pentaethylene glycol monodecyl was removed by SM-2 bio-beads
505 (Bio-Rad): five additions of bio-beads were made to the master mix every 20 minutes with
506 inversion at 4 °C: four additions of 30 mg, and the final addition of 240 mg per sample. The
507 samples were incubated overnight at 4 °C with rotation. Bio-beads were removed by passage
508 through empty micro-bio spin columns (Bio-Rad). The compound was internalized by freeze-
509 thaw-extrusion (Jaiquel Baron et al., 2021). Compound, to a final concentration of 5 mM
510 (malate and sulphate assays) or 10 mM (phosphate assays) was added, and the sample was
511 subjected to three cycles of freezing in liquid nitrogen for two minutes followed by thawing in
512 a room temperature water bath for ten minutes. Proteoliposomes were subsequently extruded
513 by 21 passages through a 0.4-µm filter (Millipore), and the external substrate was removed and
514 exchanged into buffer (20 mM HEPES, pH 7.0 and 50 mM NaCl) using a PD10 desalting column
515 (GE Healthcare) according to manufacturer's instructions.

516

517 Transport assays

518 Transport assays were performed using the Hamilton MicroLab Star robot (Hamilton Robotics
519 Ltd). Proteoliposomes (100 µL) were loaded into the wells of a MultiScreenHTS + HA 96-well
520 filter plate (pore size 0.45-µm, Millipore). Uptake of the radiolabelled substrate was initiated
521 by the addition of 100 µL buffer containing 2.5 µM [^{14}C]-malate (American Radiolabelled
522 Chemicals), 25 µM [^{35}S]-sodium sulphate (Hartmann Analytic), or 200 µM [^{33}P]-
523 orthophosphoric acid (Hartmann Analytic). Uptake was stopped after 0, 10, 20, 30, 45, 60, 150,
524 300, 450 and 600 seconds by filtration and washing three times with 200 µL ice-cold buffer (20
525 mM HEPES, pH 7.0, 50 mM NaCl). Plates were dried overnight, 200 µL MicroScint-20 (Perkin
526 Elmer) were added, and levels of radioactivity were determined using a TopCount scintillation
527 counter (Perkin Elmer). Initial rates were determined from the linear part of the uptake curve
528 (60 seconds).

529

530 SDS-PAGE analysis and protein quantification

531 Protein was visualized by SDS-PAGE analysis using 4-12% bis-tris mPAGE gels and stained using
532 InstantBlue (Abcam), according to the manufacturer's instructions. Reconstitution efficiency
533 was determined by comparing the amount of protein incorporated into proteoliposome
534 samples to a standard curve of known amounts of purified protein.

535

536 Acknowledgements

537 MSK and ACK were supported by grant MC_UU_00028/2 of the UK Medical Research Council
538 to ERSK, and EP and MRT were supported by Norwegian Research Council grant 301170 to
539 MvdG. We thank Dr. Shane Palmer (MRC Mitochondrial Biology Unit) for carrying out large-
540 scale fermentations in this project, Drs. Denis Lacabanne, Sotiria Tavoulari, Camila
541 Cimadamore-Werthein and Pavel Dolezal for constructive comments on the manuscript, and
542 Associate Professor Kevin S. W. Tan for the ST7-B *Blastocystis* culture.

543

544 Author contributions

545 Conception and design of the research: E.P., M.S.K., M.v.d.G., and E.R.S.K.
546 Bioinformatic analyses: A.C.K. and E.P.
547 Molecular biology: M.S.K.

548 Microscopy: M.R.T.

549 Protein purification and thermostability analyses: E.P.

550 Transport assays: E.P., and M.S.K.

551 Data analysis: E.P. and M.S.K.

552 Data interpretation: E.P., M.S.K., M.v.d.G., and E.R.S.K.

553 Writing of the paper: E.P., M.S.K., A.C.K., M.R.T., M.v.d.G., and E.R.S.K

554 All authors read and revised the paper.

555

556 Competing financial interests

557 The authors declare no competing interests.

558 References

559 Abrahamian, M., Kagda, M., Ah-Fong, A.M.V., and Judelson, H.S. (2017). Rethinking the
560 evolution of eukaryotic metabolism: novel cellular partitioning of enzymes in stramenopiles
561 links serine biosynthesis to glycolysis in mitochondria. BMC Evol Biol *17*, 241.
562 Ajjampur, S.S., Png, C.W., Chia, W.N., Zhang, Y., and Tan, K.S. (2016). Ex Vivo and In Vivo Mice
563 Models to Study Blastocystis spp. Adhesion, Colonization and Pathology: Closer to Proving
564 Koch's Postulates. PLoS One *11*, e0160458.
565 Alexander, C.G., Wanner, R., Johnson, C.M., Breitsprecher, D., Winter, G., Duhr, S., Baaske, P.,
566 and Ferguson, N. (2014). Novel microscale approaches for easy, rapid determination of
567 protein stability in academic and commercial settings. Biochim Biophys Acta *1844*, 2241-2250.
568 Andersen, L.O., Bonde, I., Nielsen, H.B., and Stensvold, C.R. (2015). A retrospective
569 metagenomics approach to studying Blastocystis. FEMS Microbiol Ecol *91*.
570 Andersen, L.O., and Stensvold, C.R. (2016). Blastocystis in Health and Disease: Are We Moving
571 from a Clinical to a Public Health Perspective? J Clin Microbiol *54*, 524-528.
572 Audebert, C., Even, G., Cian, A., Blastocystis Investigation, G., Loywick, A., Merlin, S.,
573 Viscogliosi, E., and Chabe, M. (2016). Colonization with the enteric protozoa Blastocystis is
574 associated with increased diversity of human gut bacterial microbiota. Sci Rep *6*, 25255.
575 Bártulos, R.C., Rogers, M.B., Williams, T.A., Gentekaki, E., Brinkmann, H., Cerff, R., Liaud, M.F.,
576 Hehl, A.B., Yarlett, N.R., Gruber, A.*, et al.* (2018). Mitochondrial Glycolysis in a Major Lineage
577 of Eukaryotes. Genome Biol Evol *10*, 2310-2325.
578 Bisaccia, F., Indiveri, C., and Palmieri, F. (1988). Purification and reconstitution of two anion
579 carriers from rat liver mitochondria: the dicarboxylate and the 2-oxoglutarate carrier. Biochim
580 Biophys Acta *933*, 229-240.
581 Bricker, D.K., Taylor, E.B., Schell, J.C., Orsak, T., Boutron, A., Chen, Y.C., Cox, J.E., Cardon, C.M.,
582 Van Vranken, J.G., Dephoure, N.*, et al.* (2012). A mitochondrial pyruvate carrier required for
583 pyruvate uptake in yeast, Drosophila, and humans. Science *337*, 96-100.
584 Bruno, S., Pinto, A., Paredi, G., Tamborini, L., De Micheli, C., La Pietra, V., Marinelli, L.,
585 Novellino, E., Conti, P., and Mozzarelli, A. (2014). Discovery of covalent inhibitors of
586 glyceraldehyde-3-phosphate dehydrogenase, a target for the treatment of malaria. J Med
587 Chem *57*, 7465-7471.
588 Burki, F., Roger, A.J., Brown, M.W., and Simpson, A.G.B. (2020). The New Tree of Eukaryotes.
589 Trends Ecol Evol *35*, 43-55.

590 Castegna, A., Scarcia, P., Agrimi, G., Palmieri, L., Rottensteiner, H., Spera, I., Germinario, L.,
591 and Palmieri, F. (2010). Identification and functional characterization of a novel mitochondrial
592 carrier for citrate and oxoglutarate in *Saccharomyces cerevisiae*. J Biol Chem *285*, 17359-
593 17370.
594 Crichton, P.G., Lee, Y., Ruprecht, J.J., Cerson, E., Thangaratnarajah, C., King, M.S., and Kunji,
595 E.R. (2015). Trends in thermostability provide information on the nature of substrate,
596 inhibitor, and lipid interactions with mitochondrial carriers. J Biol Chem *290*, 8206-8217.
597 Crompton, M., Palmieri, F., Capano, M., and Quagliariello, E. (1974). The transport of
598 thiosulphate in rat liver mitochondria. FEBS Lett *46*, 247-250.
599 Deng, L., Lee, J.W.J., and Tan, K.S.W. (2022). Infection with pathogenic Blastocystis ST7 is
600 associated with decreased bacterial diversity and altered gut microbiome profiles in diarrheal
601 patients. Parasit Vectors *15*, 312.
602 Deng, L., Wojciech, L., Png, C.W., Kioh, D.Y.Q., Gu, Y., Aung, T.T., Malleret, B., Chan, E.C.Y.,
603 Peng, G., Zhang, Y.*, et al.* (2023). Colonization with two different Blastocystis subtypes in DSS-
604 induced colitis mice is associated with strikingly different microbiome and pathological
605 features. Theranostics *13*, 1165-1179.
606 Denoeud, F., Roussel, M., Noel, B., Wawrzyniak, I., Da Silva, C., Diogon, M., Viscogliosi, E.,
607 Brochier-Armanet, C., Couloux, A., Poulain, J.*, et al.* (2011). Genome sequence of the
608 stramenopile Blastocystis, a human anaerobic parasite. Genome Biol *12*, R29.
609 Dogruman-Al, F., Kustimur, S., Yoshikawa, H., Tuncer, C., Simsek, Z., Tanyuksel, M., Araz, E.,
610 and Boorom, K. (2009). Blastocystis subtypes in irritable bowel syndrome and inflammatory
611 bowel disease in Ankara, Turkey. Mem Inst Oswaldo Cruz *104*, 724-727.
612 Fiermonte, G., Dolce, V., Palmieri, L., Ventura, M., Runswick, M.J., Palmieri, F., and Walker, J.E.
613 (2001). Identification of the human mitochondrial oxodicarboxylate carrier. Bacterial
614 expression, reconstitution, functional characterization, tissue distribution, and chromosomal
615 location. J Biol Chem *276*, 8225-8230.
616 Fiermonte, G., Walker, J.E., and Palmieri, F. (1993). Abundant bacterial expression and
617 reconstitution of an intrinsic membrane-transport protein from bovine mitochondria.
618 Biochem J *294*, 293-299.
619 Gentekaki, E., Curtis, B.A., Stairs, C.W., Klimes, V., Elias, M., Salas-Leiva, D.E., Herman, E.K.,
620 Eme, L., Arias, M.C., Henrissat, B.*, et al.* (2017). Extreme genome diversity in the hyper-
621 prevalent parasitic eukaryote Blastocystis. PLoS Biol *15*, e2003769.

622 Haresh, K., Suresh, K., Khairul Anus, A., and Saminathan, S. (1999). Isolate resistance of
623 Blastocystis hominis to metronidazole. Trop Med Int Health *4*, 274-277.
624 Herzig, S., Raemy, E., Montessuit, S., Veuthey, J.L., Zamboni, N., Westermann, B., Kunji, E.R.,
625 and Martinou, J.C. (2012). Identification and functional expression of the mitochondrial
626 pyruvate carrier. Science *337*, 93-96.
627 Hoang, D.T., Chernomor, O., von Haeseler, A., Minh, B.Q., and Vinh, L.S. (2018). UFBoot2:
628 Improving the Ultrafast Bootstrap Approximation. Mol Biol Evol *35*, 518-522.
629 Jaiquel Baron, S., King, M.S., Kunji, E.R.S., and Schirris, T.J.J. (2021). Characterization of drug-
630 induced human mitochondrial ADP/ATP carrier inhibition. Theranostics *11*, 5077-5091.
631 Jiang, R.H., and Tyler, B.M. (2012). Mechanisms and evolution of virulence in oomycetes. Annu
632 Rev Phytopathol *50*, 295-318.
633 Jones, P., Binns, D., Chang, H.Y., Fraser, M., Li, W., McAnulla, C., McWilliam, H., Maslen, J.,
634 Mitchell, A., Nuka, G.*, et al.* (2014). InterProScan 5: genome-scale protein function
635 classification. Bioinformatics *30*, 1236-1240.
636 King, M.S., and Kunji, E.R.S. (2020). Expression and purification of membrane proteins in
637 *Saccharomyces cerevisiae*. Methods Mol Biol *2127*, 47-61.
638 Kunji, E.R.S., King, M.S., Ruprecht, J.J., and Thangaratnarajah, C. (2020). The SLC25 Carrier
639 Family: Important Transport Proteins in Mitochondrial Physiology and Pathology. Physiology
640 (Bethesda) *35*, 302-327.
641 Kunji, E.R.S., and Robinson, A.J. (2006). The conserved substrate binding site of mitochondrial
642 carriers. Biochim Biophys Acta *1757*, 1237-1248.
643 Lantsman, Y., Tan, K.S.W., Morada, M., and Yarlett, N. (2008). Biochemical characterization of
644 a mitochondrial-like organelle from Blastocystis sp. subtype 7. Microbiology (Reading) *154*,
645 2757-2766.
646 Leonardi, S.S., Li, F.J., Chee, M.S., Yason, J.A., Tay, H.Y., Chen, J.Y., Koh, E.Y., He, C.Y., and Tan,
647 K.S. (2021). Characterisation of novel functionality within the Blastocystis tryptophanase
648 gene. PLoS Negl Trop Dis *15*, e0009730.
649 Majd, H., King, M.S., Palmer, S.M., Smith, A.C., Elbourne, L.D., Paulsen, I.T., Sharples, D.,
650 Henderson, P.J., and Kunji, E.R. (2018). Screening of candidate substrates and coupling ions of
651 transporters by thermostability shift assays. Elife *7*, e38821.

652 Mavridou, V., King, M.S., Tavoulari, S., Ruprecht, J.J., Palmer, S.M., and Kunji, E.R.S. (2022).
653 Substrate binding in the mitochondrial ADP/ATP carrier is a step-wise process guiding the
654 structural changes in the transport cycle. Nat Commun *13*, 3585.
655 McNae, I.W., Kinkead, J., Malik, D., Yen, L.H., Walker, M.K., Swain, C., Webster, S.P., Gray, N.,
656 Fernandes, P.M., Myburgh, E.*, et al.* (2021). Fast acting allosteric phosphofructokinase
657 inhibitors block trypanosome glycolysis and cure acute African trypanosomiasis in mice. Nat
658 Commun *12*, 1052.
659 Minh, B.Q., Schmidt, H.A., Chernomor, O., Schrempf, D., Woodhams, M.D., von Haeseler, A.,
660 and Lanfear, R. (2020). IQ-TREE 2: New Models and Efficient Methods for Phylogenetic
661 Inference in the Genomic Era. Mol Biol Evol *37*, 1530-1534.
662 Mirza, H., Teo, J.D., Upcroft, J., and Tan, K.S. (2011). A rapid, high-throughput viability assay
663 for Blastocystis spp. reveals metronidazole resistance and extensive subtype-dependent
664 variations in drug susceptibilities. Antimicrob Agents Chemother *55*, 637-648.
665 Moghaddam, D.D., Ghadirian, E., and Azami, M. (2005). Blastocystis hominis and the
666 evaluation of efficacy of metronidazole and trimethoprim/sulfamethoxazole. Parasitol Res *96*,
667 273-275.
668 Müller, M., Mentel, M., van Hellemond, J.J., Henze, K., Woehle, C., Gould, S.B., Yu, R.Y., van
669 der Giezen, M., Tielens, A.G., and Martin, W.F. (2012). Biochemistry and evolution of
670 anaerobic energy metabolism in eukaryotes. Microbiol Mol Biol Rev *76*, 444-495.
671 Nakayama, T., Ishida, K., and Archibald, J.M. (2012). Broad distribution of TPI-GAPDH fusion
672 proteins among eukaryotes: evidence for glycolytic reactions in the mitochondrion? PLoS One
673 *7*, e52340.
674 Opperdoes, F.R., and Borst, P. (1977). Localization of nine glycolytic enzymes in a microbody-
675 like organelle in Trypanosoma brucei: the glycosome. FEBS Lett *80*, 360-364.
676 Palmieri, F., Quagliariello, E., and Klingenberger, M. (1972). Kinetics and specificity of the
677 oxoglutarate carrier in rat-liver mitochondria. Eur J Biochem *29*, 408-416.
678 Penna-Coutinho, J., Cortopassi, W.A., Oliveira, A.A., Franca, T.C., and Krettli, A.U. (2011).
679 Antimalarial activity of potential inhibitors of Plasmodium falciparum lactate dehydrogenase
680 enzyme selected by docking studies. PLoS One *6*, e21237.
681 Picault, N., Palmieri, L., Pisano, I., Hodges, M., and Palmieri, F. (2002). Identification of a novel
682 transporter for dicarboxylates and tricarboxylates in plant mitochondria. Bacterial expression,

683 reconstitution, functional characterization, and tissue distribution. J Biol Chem *277*, 24204-
684 24211.
685 Poirier, P., Wawrzyniak, I., Vivares, C.P., Delbac, F., and El Alaoui, H. (2012). New insights into
686 Blastocystis spp.: a potential link with irritable bowel syndrome. PLoS Pathog *8*, e1002545.
687 Priyam, A., Woodcroft, B.J., Rai, V., Moghul, I., Munagala, A., Ter, F., Chowdhary, H., Pieniak,
688 I., Maynard, L.J., Gibbins, M.A.*, et al.* (2019). Sequenceserver: A Modern Graphical User
689 Interface for Custom BLAST Databases. Mol Biol Evol *36*, 2922-2924.
690 Ravindra, G., and Balaram, P. (2005). Plasmodium falciparum triosephosphate isomerase: New
691 insights into an old enzyme. Pure Appl Chem *77*, 281-289.
692 Robinson, A.J., and Kunji, E.R.S. (2006). Mitochondrial carriers in the cytoplasmic state have a
693 common substrate binding site. Proc Natl Acad Sci USA *103*, 2617-2622.
694 Ruprecht, J.J., King, M.S., Zogg, T., Aleksandrova, A.A., Pardon, E., Crichton, P.G., Steyaert, J.,
695 and Kunji, E.R.S. (2019). The molecular mechanism of transport by the mitochondrial ADP/ATP
696 carrier. Cell *176*, 435-447.
697 Ruprecht, J.J., and Kunji, E.R.S. (2020). The SLC25 mitochondrial carrier family: structure and
698 mechanism. Trends Biochem Sci *45*, 244-258.
699 Ruprecht, J.J., and Kunji, E.R.S. (2021). Structural Mechanism of Transport of Mitochondrial
700 Carriers. Annu Rev Biochem *90*, 535-558.
701 Saraste, M., and Walker, J.E. (1982). Internal sequence repeats and the path of polypeptide in
702 mitochondrial ADP/ATP translocase. FEBS Lett *144*, 250-254.
703 Saris, N.E.L. (1980). Sulfate transport by H+ symport and by the dicarboxylate carrier in
704 mitochondria. Biochem J *192*, 911-917.
705 Stechmann, A., Hamblin, K., Perez-Brocal, V., Gaston, D., Richmond, G.S., van der Giezen, M.,
706 Clark, C.G., and Roger, A.J. (2008). Organelles in Blastocystis that blur the distinction between
707 mitochondria and hydrogenosomes. Curr Biol *18*, 580-585.
708 Stensvold, C.R., Berg, R., Maloney, J.G., Molokin, A., and Santin, M. (2023). Molecular
709 characterization of *Blastocystis* and *Entamoeba* of muskoxen and sheep in Greenland. Int J
710 Parasitol *53*, 673-685.
711 Stensvold, C.R., Lewis, H.C., Hammerum, A.M., Porsbo, L.J., Nielsen, S.S., Olsen, K.E., Arendrup,
712 M.C., Nielsen, H.V., and Molbak, K. (2009). Blastocystis: unravelling potential risk factors and
713 clinical significance of a common but neglected parasite. Epidemiol Infect *137*, 1655-1663.

714 Stensvold, C.R., Sorland, B.A., Berg, R., Andersen, L.O., van der Giezen, M., Bowtell, J.L., El-
715 Badry, A.A., Belkessa, S., Kurt, O., and Nielsen, H.V. (2022). Stool Microbiota Diversity Analysis
716 of Blastocystis-Positive and Blastocystis-Negative Individuals. Microorganisms *10*.
717 Stensvold, C.R., and van der Giezen, M. (2018). Associations between Gut Microbiota and
718 Common Luminal Intestinal Parasites. Trends Parasitol *34*, 369-377.
719 Stenzel, D.J., and Boreham, P.F. (1996). Blastocystis hominis revisited. Clin Microbiol Rev *9*,
720 563-584.
721 Tavoulari, S., Schirris, T.J.J., Mavridou, V., Thangaratnarajah, C., King, M.S., Jones, D.T.D., Ding,
722 S., Fearnley, I.M., and Kunji, E.R.S. (2022). Key features of inhibitor binding to the human
723 mitochondrial pyruvate carrier hetero-dimer. Mol Metab, 101469.
724 Tito, R.Y., Chaffron, S., Caenepeel, C., Lima-Mendez, G., Wang, J., Vieira-Silva, S., Falony, G.,
725 Hildebrand, F., Darzi, Y., Rymenans, L.*, et al.* (2019). Population-level analysis of Blastocystis
726 subtype prevalence and variation in the human gut microbiota. Gut *68*, 1180-1189.
727 Toleco, M.R., Naake, T., Zhang, Y., Heazlewood, J.L., and Fernie, A.R. (2020). Plant
728 Mitochondrial Carriers: Molecular Gatekeepers That Help to Regulate Plant Central Carbon
729 Metabolism. Plants (Basel) *9*.
730 Tsaousis, A.D., Hamblin, K.A., Elliott, C.R., Young, L., Rosell-Hidalgo, A., Gourlay, C.W., Moore,
731 A.L., and van der Giezen, M. (2018). The Human Gut Colonizer Blastocystis Respires Using
732 Complex II and Alternative Oxidase to Buffer Transient Oxygen Fluctuations in the Gut. Front
733 Cell Infect Microbiol *8*, 371.
734 Wawrzyniak, I., Roussel, M., Diogon, M., Couloux, A., Texier, C., Tan, K.S., Vivares, C.P., Delbac,
735 F., Wincker, P., and El Alaoui, H. (2008). Complete circular DNA in the mitochondria-like
736 organelles of Blastocystis hominis. Int J Parasitol *38*, 1377-1382.
737 Wu, Z., Mirza, H., and Tan, K.S. (2014). Intra-subtype variation in enteroadhesion accounts for
738 differences in epithelial barrier disruption and is associated with metronidazole resistance in
739 Blastocystis subtype-7. PLoS Negl Trop Dis *8*, e2885.
740 Yason, J.A., Liang, Y.R., Png, C.W., Zhang, Y., and Tan, K.S.W. (2019). Interactions between a
741 pathogenic Blastocystis subtype and gut microbiota: in vitro and in vivo studies. Microbiome
742 *7*, 30.
743 Zhou, L., Maldonado, M., Padavannil, A., Guo, F., and Letts, J.A. (2022). Structures of
744 Tetrahymena's respiratory chain reveal the diversity of eukaryotic core metabolism. Science
745 *376*, 831-839.

746 Zierdt, C.H. (1991). Blastocystis hominis--past and future. Clin Microbiol Rev *4*, 61-79.
747 Zierdt, C.H., Donnolley, C.T., Muller, J., and Constantopoulos, G. (1988). Biochemical and
748 ultrastructural study of Blastocystis hominis. J Clin Microbiol *26*, 965-970.
749

Figures and legends

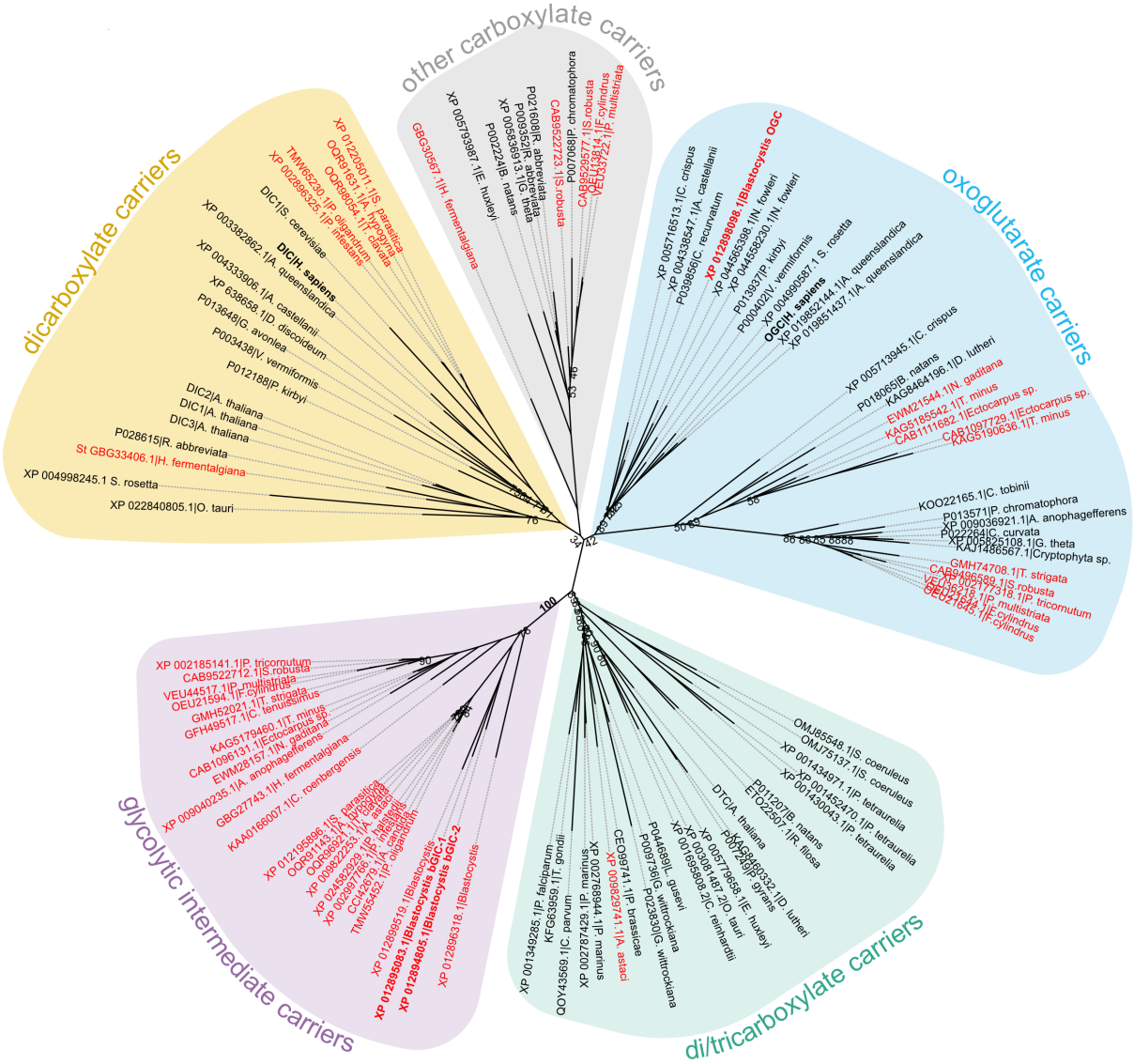

Figure 1: Phylogenetic analysis of carboxylate carriers. The maximum likelihood tree was generated by IQ-TREE with the LG + F + R7 model suggested by ModelFinder. The support was calculated using ultrafast bootstrap analysis. The unrooted phylogenetic tree shows the uniqueness of the identified putative stramenopile glycolytic intermediate carriers amongst eukaryotes. The stramenopile-specific glycolytic intermediate carriers (GIC - pink) are most closely related to di/tricarboxylate carriers (DTC – green), and to a lesser extend to oxoglutarate carriers (OGC - blue) and dicarboxylate carriers (DIC - yellow). Stramenopile proteins are in red, proteins included in this study are in bold. Note the absence of any non-stramenopile sequences in this clade. Bootstrap values less than 90 and a value for the GIC group are indicated.

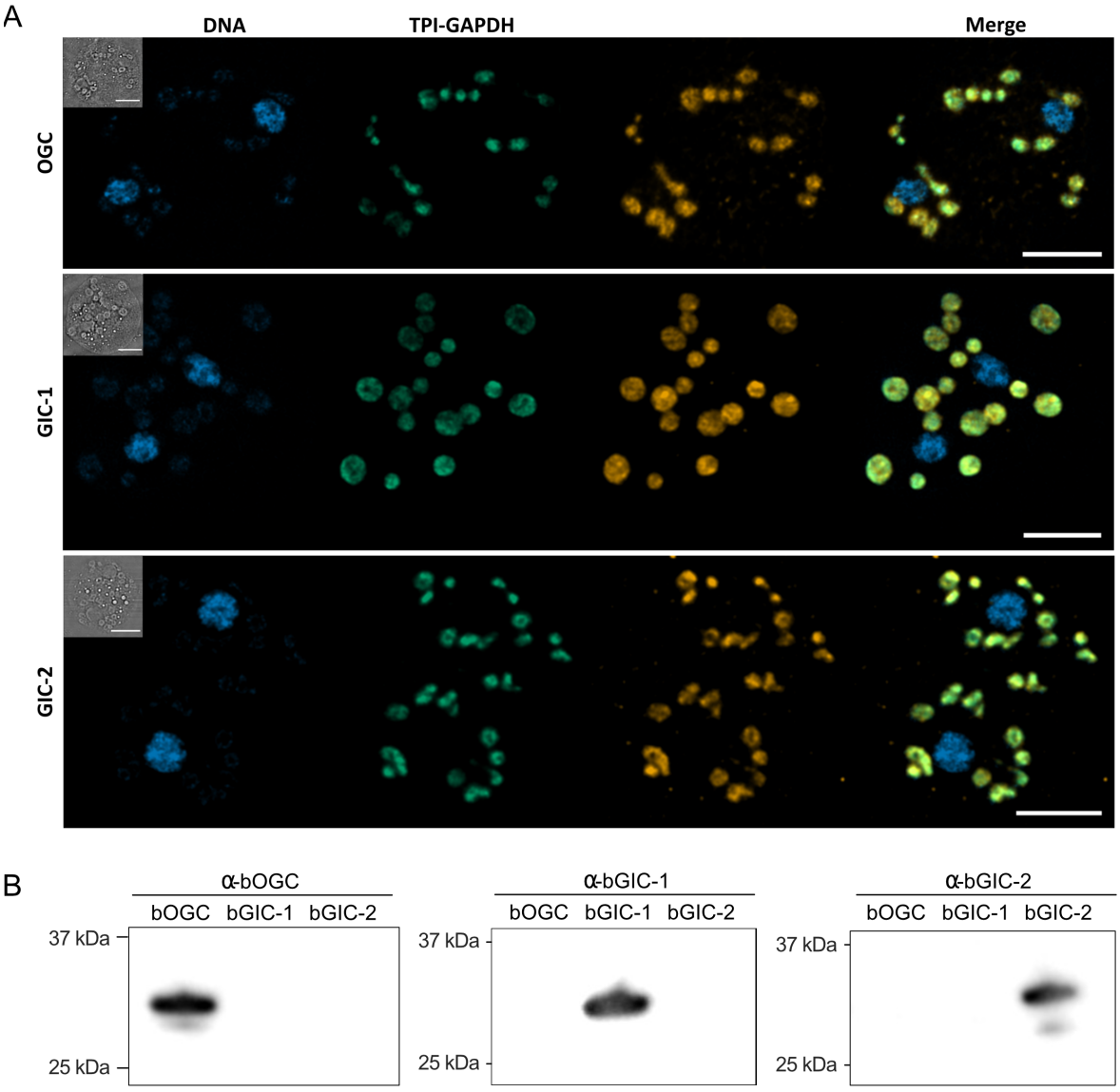

Figure 2: A) Localisation of GIC carriers in *Blastocystis* ST7-B cells using specific antibodies (orange). The signal colocalises with the mitochondrial protein TPI-GAPDH (green) (Bártulos et al., 2018), demonstrating its mitochondrial localisation. DNA is stained with Hoechst 33342 (blue). Inserts top left: corresponding brightfield image. The scale bar is 5 μm. **B**) Western blots of *Blastocystis* OGC, GIC-1, and GIC-2 antibodies against purified protein confirm that there is no cross reactivity.

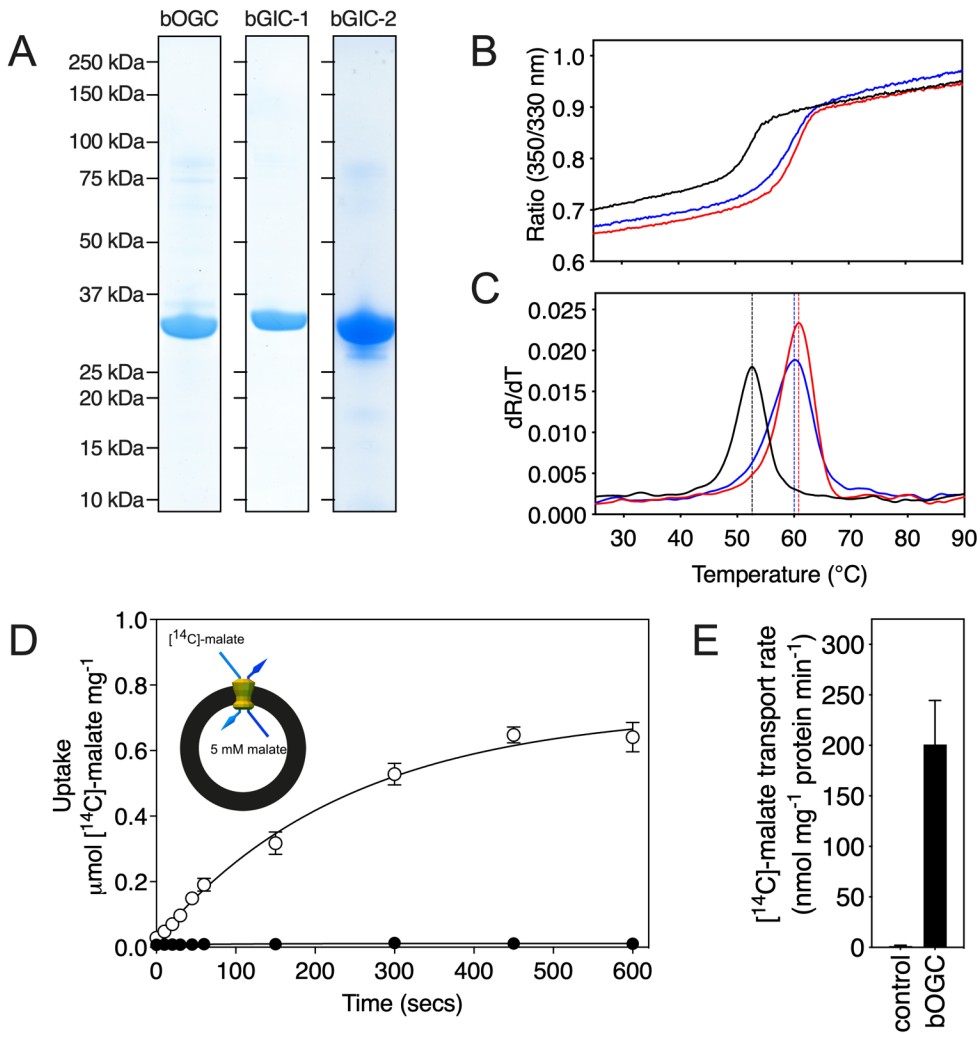

Figure 3: Expression, purification and biophysical characterization of *Blastocystis* carriers. **A**) Instant-blue stained SDS-PAGE gel of purified bOGC, bGIC-1 and bGIC-2. **B**) Typical unfolding curves of bOGC (black trace), bGIC-1 (red trace), and bGIC-2 (blue trace) using nanoDSF. **C**) The peak in the derivative of the unfolding curve (dR/dT) is the apparent melting temperature (Tm). **D**) [^{14}C]-malate uptake curve of bOGC reconstituted into proteoliposomes loaded with (white circles) or without (black circles) 5 mM malate. Transport was initiated by the external addition of 2.5 µM [^{14}C]-malate. **E**) Initial transport rates, calculated from panel **D**) from the linear part of the uptake curve (first 60 seconds). The data represent the mean and standard deviation is of n=4 (two biological repeats, each with two technical repeats).

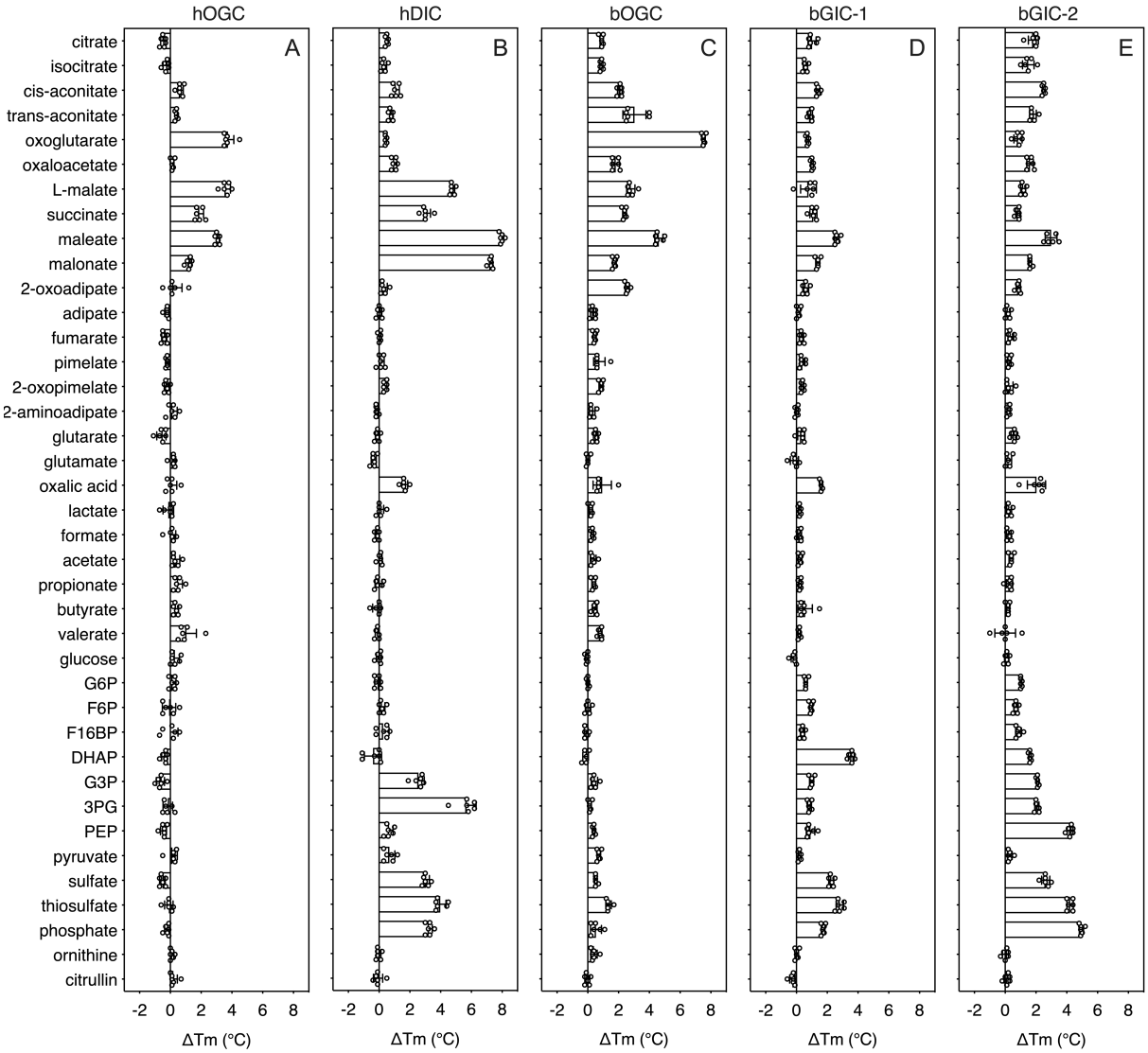

783

784

785 **Figure 4:** Thermostability screening of detergent-solubilized, purified protein using nanoDSF
786 (Prometheus, Nanotemper). **A**) hOGC, **B**) hDIC, **C**) bOGC, **D**) bGIC-1, and **E**) bGIC-2 against 10
787 mM di- and tricarboxylates, glycolytic intermediates and inorganic ions. The temperature shift
788 (ΔTm) is the apparent melting temperature in the presence of compound minus the apparent
789 melting temperature in the absence of compound. The data are represented by the mean and
790 standard deviation of two biological repeats, each in triplicate (n=6 in total). G6P, glucose-6-
791 phosphate; F6P, fructose-6-phosphate; F16BP, fructose 1-6 bisphosphate; DHAP,
792 dihydroxyacetone phosphate; G3P, glyceraldehyde-3-phosphate; 3PG, 3-phosphoglycerate;
793 PEP, phosphoenolpyruvate.

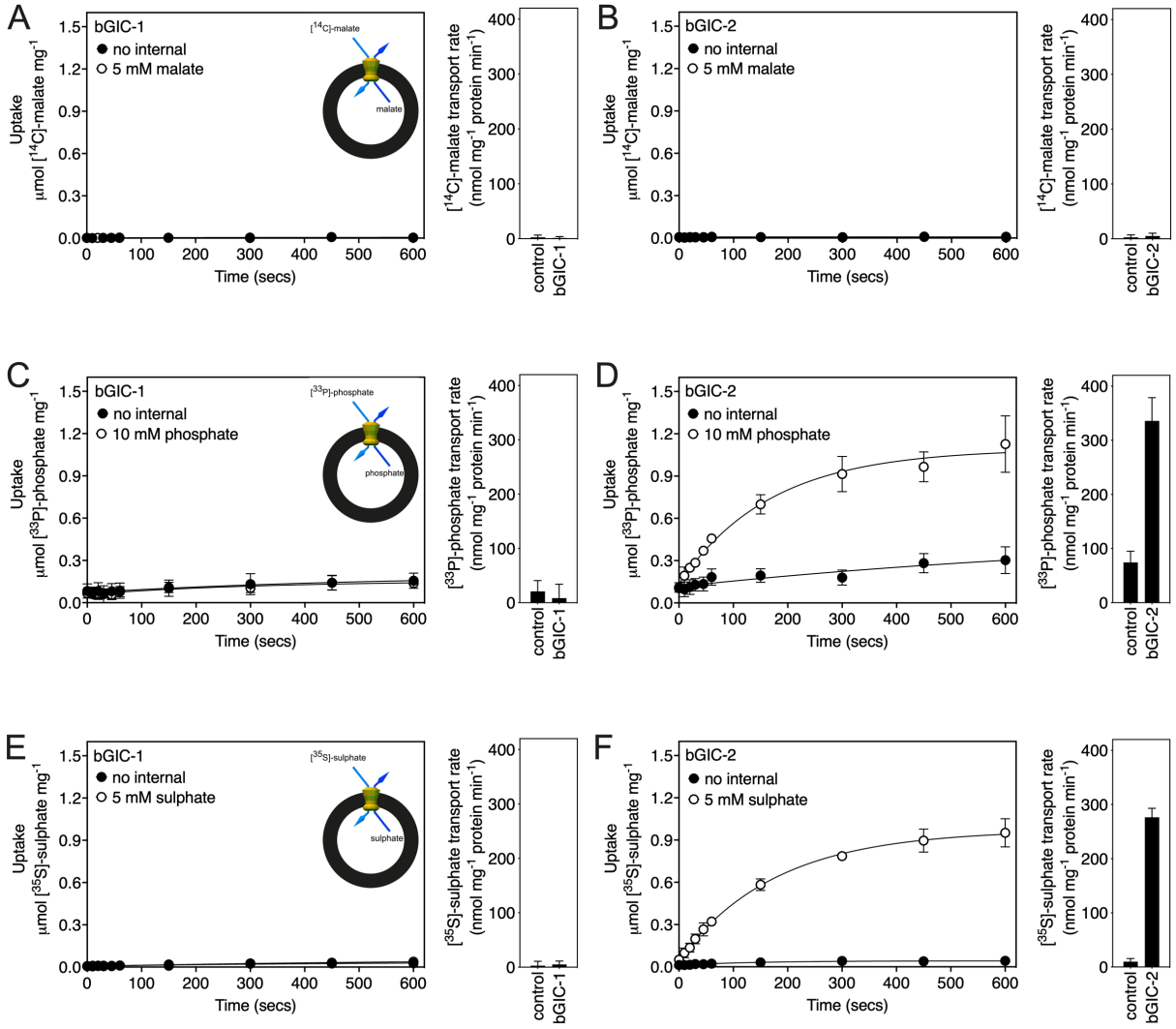

Figure 5: Proteoliposomes containing *Blastocystis* putative glycolytic intermediate carriers 1 (bGIC-1; **A**, **C** and **E**) and 2 (bGIC-2; **B**, **D** and **F**) were loaded with either (**A** and **B**) 5 mM malate, (**C** and **D**) 10 mM phosphate or (**E** and **F**) 5 mM sodium sulphate, and transport initiated by the external addition of (**A** and **B**) 2.5 µM [^{14}C]-malate, (**C** and **D**) 200 µM [^{33}P]-phosphate or (**E** and **F**) 25 µM [^{35}S]-sulphate. Controls with no internalized substrate were also tested (black circles). Initial transport rates were calculated from the linear part of the uptake curve (60 seconds). The data represent the mean and standard deviation of two biological repeats, each with two technical repeats (n=4 in total).

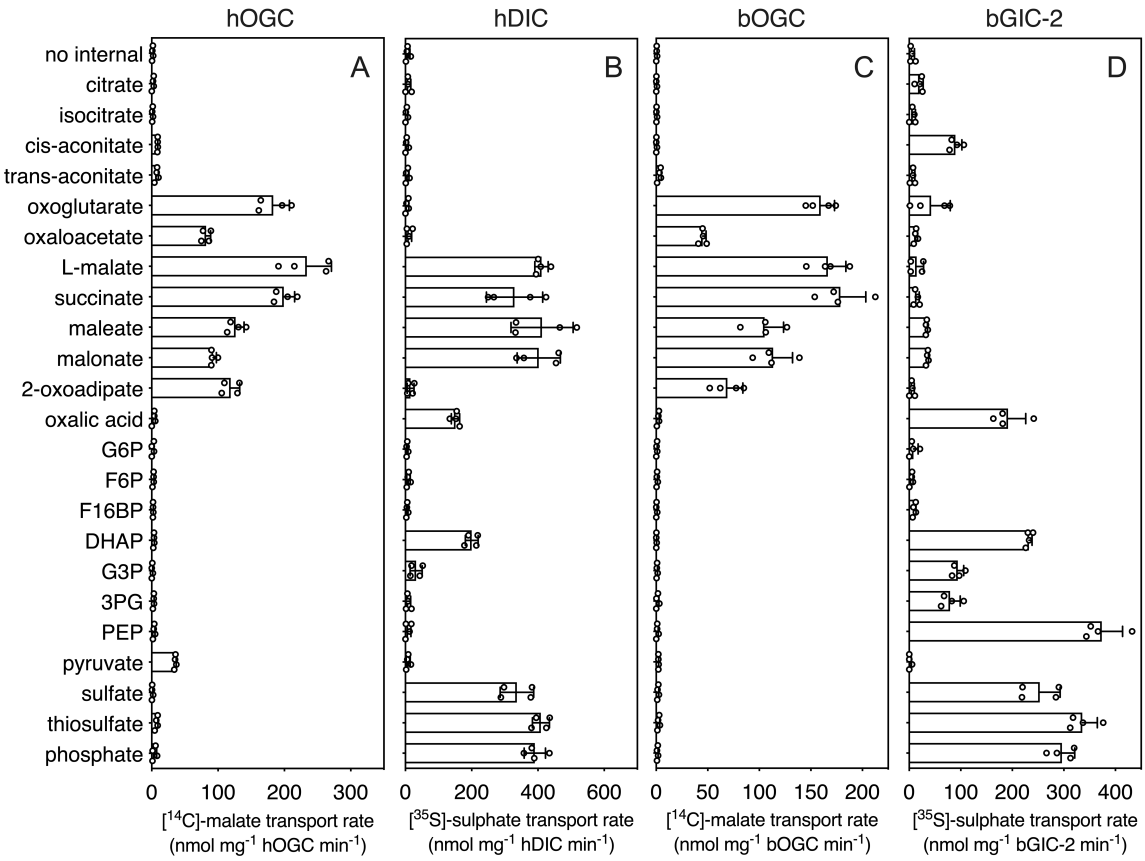

Figure 6: Hetero-exchange reactions catalysed by reconstituted carriers. **A**) Proteoliposomes containing human oxoglutarate carrier (hOGC, SLC25A11), **B**) human dicarboxylate carrier (hDIC, SLC25A10), **C**) *Blastocystis* oxoglutarate carrier (bOGC) and **D**) *Blastocystis* putative glycolytic intermediate carrier 2 (bGIC-2) were loaded with 5 mM compound, and transport initiated by the external addition of 2.5 µM [^{14}C]-malate (hOGC and bOGC) or 25 µM [^{35}S]-sulphate (hDIC and bGIC-2). Initial transport rates were calculated from the linear part of the uptake curve (60 seconds). The data represent the mean and standard deviation of two biological repeats, each with two technical repeats (n=4 in total). G6P, glucose-6-phosphate; F6P, fructose-6-phosphate; F16BP, fructose 1-6 bisphosphate; DHAP, dihydroxyacetone phosphate; G3P, glyceraldehyde-3-phosphate; 3PG, 3-phosphoglycerate; PEP, phosphoenolpyruvate.

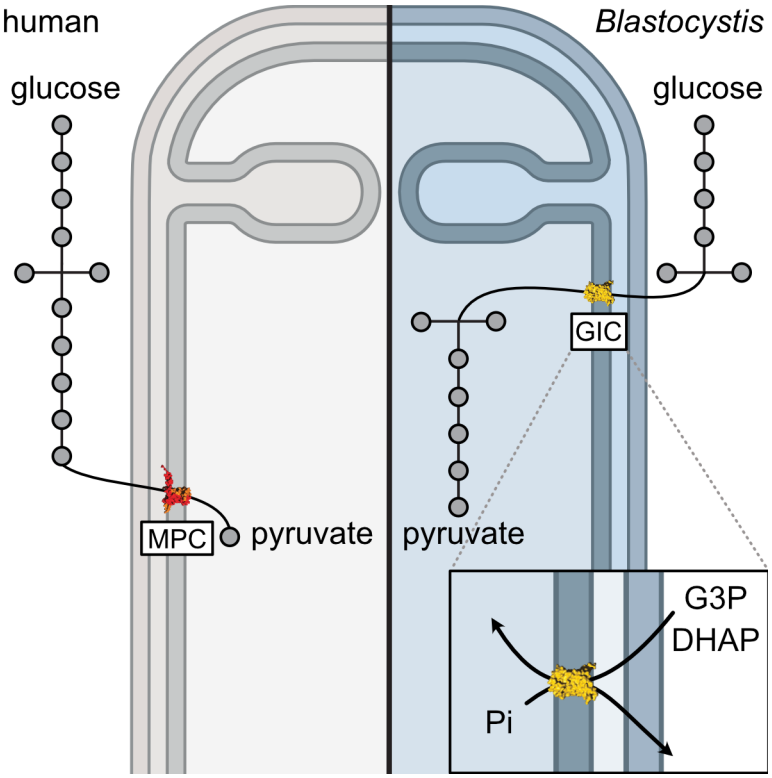

Figure 7: Comparing glycolysis in humans and *Blastocystis*.

other carboxylate carriers
dicarboxylate carriers
oxoglutarate carriers
glycolytic intermediate carriers
di/tricarboxylate carriers
XP 012205011.1|S. parasitica
OQR91631.1|A. hypogyna
OQR98054.1|T. clavata
TMW65230.1|P. oligandrum
XP 002896325.1|P. infestans
DIC1|S. cerevisiae
DIC|H. sapiens
XP 003382862.1|A. queenslandica
XP 004333906.1|A. castellanii
XP 638658.1|D. discoideum
P013648|G. avonlea
P003438|V. vermiformis
P012188|P. kirbyi
DIC2|A. thaliana
DIC1|A. thaliana
DIC3|A. thaliana
P028615|R. abbreviata
St GBG33406.1|H. fermentalgiana
XP 004998245.1 S. rosetta
XP 022840805.1|O. tauri
XP 005793987.1|E. huxleyi
GBG30567.1|H. fermentalgiana
P002224|B. natans
XP 005836913.1|G. theta
P009352|R. abbreviata
P021608|R. abbreviata
CAB9522723.1|S.robusta
P007068|P. chromatophora
CAB9529577.1|S.robusta
VEU13814.1|F.cylindrus
VEU33722.1|P. multistriata
XP 005716513.1|C. crispus
XP 004338547.1|A. castellanii
P039856|C. recurvatum
XP 012898098.1|Blastocystis OGC
XP 044565398.1|N. fowleri
XP 044558230.1|N. fowleri
P013937|P. kirbyi
P000402|V. vermiformis
XP 004990587.1 S. rosetta
OGC|H. sapiens
XP 019852144.1|A. queenslandica
XP 019851437.1|A. queenslandica
XP 005713945.1|C. crispus
P018065|B. natans
KAG8464196.1|D. lutheri
EWM21544.1|N. gaditana
KAG5185542.1|T. minus
CAB1111682.1|Ectocarpus sp.
CAB1097729.1|Ectocarpus sp.
KAG5190636.1|T. minus
KOO22165.1|C. tobinii
P013571|P. chromatophora
XP 009036921.1|A. anophagefferens
P022264|C. curvata
XP 005825108.1|G. theta
KAJ1486567.1|Cryptophyta sp.
GMH74708.1|T. strigata
CAB9496589.1|S.robusta
XP 002177318.1|P. tricornutum
VEU36218.1|P. multistriata
OEU21644.1|F.cylindrus
OEU21645.1|F.cylindrus
XP 002185141.1|P. tricornutum
CAB9522712.1|S.robusta
VEU44517.1|P. multistriata
OEU21594.1|F.cylindrus
GMH52021.1|T. strigata
GFH49517.1|C. tenuissimus
KAG5179460.1|T. minus
CAB1096131.1|Ectocarpus sp.
EWM28157.1|N. gaditana
XP 009040235.1|A. anophagefferens
GBG27743.1|H. fermentalgiana
KAA0166007.1|C. roenbergensis
XP 012195896.1|S. parasitica
OQR91143.1|A. hypogyna
OQR96921.1|T. clavata
XP 009822253.1|A. astaci
XP 024582929.1|P. halstedii
XP 002997766.1|P. infestans
CCI42679.1|A. candida
TMW55452.1|P. oligandrum
XP 012899519.1|Blastocystis
XP 012895083.1|Blastocystis bGIC-1
XP 012894805.1|Blastocystis bGIC-2
XP 012896318.1|Blastocystis
OMJ85548.1|S. coeruleus
OMJ75137.1|S. coeruleus
XP 001434971.1|P. tetraurelia
XP 001452470.1|P. tetraurelia
XP 001430043.1|P. tetraurelia
P011207|B. natans
ETO22507.1|R. filosa
DTC|A. thaliana
KAG8460332.1|D. lutheri
P007249|P. gyrans
XP 005779658.1|E. huxleyi
XP 003081487.2|O. tauri
XP 001695808.2|C. reinhardtii
P044689|L. gusevi
P009736|G. wittrockiana
P023830|G. wittrockiana
CEO99741.1|P. brassicae
XP 009829741.1|A. astaci
XP 002768944.1|P. marinus
XP 002787429.1|P. marinus
QOY43569.1|C. parvum
KFG63959.1|T. gondii
XP 001349285.1|P. falciparum

A

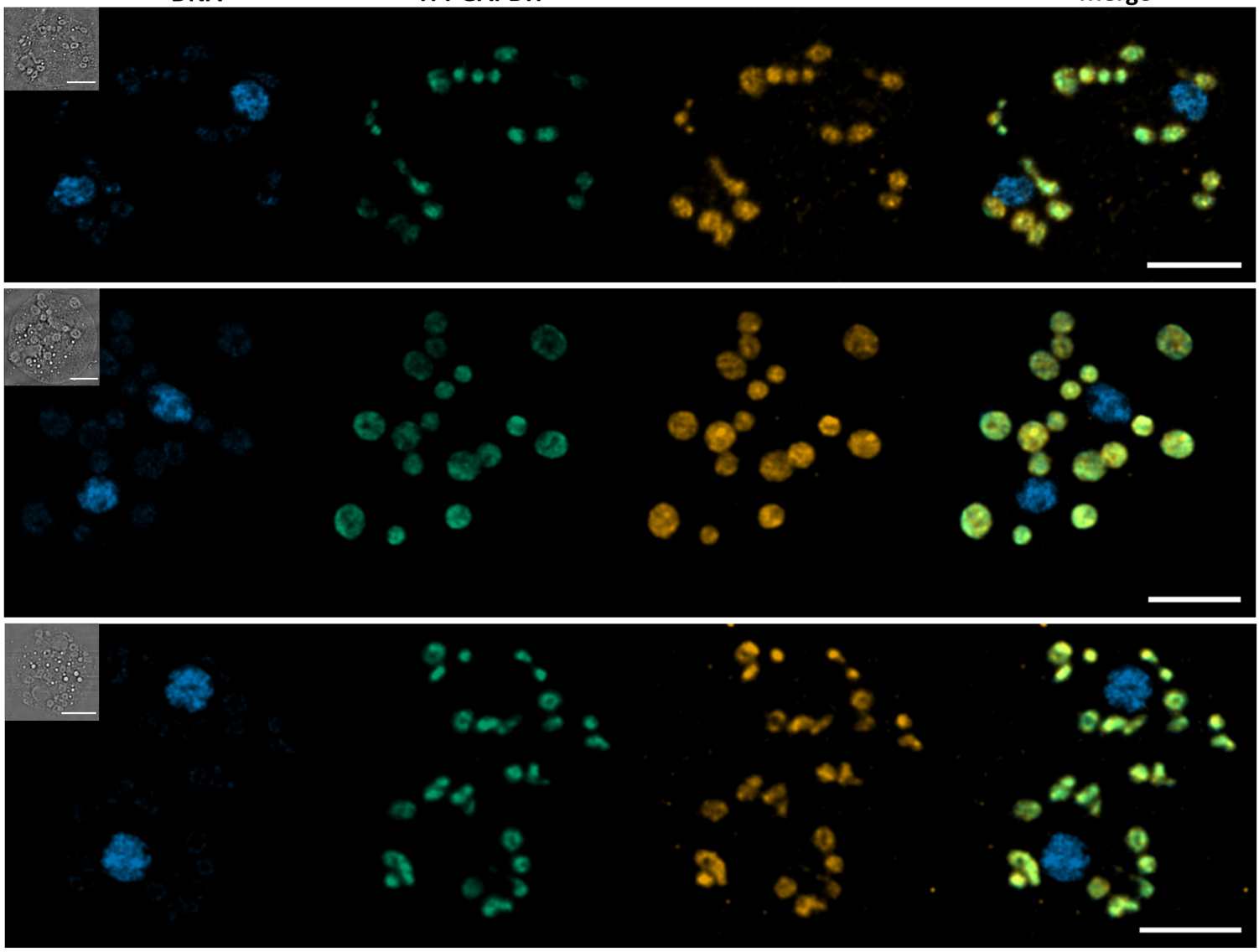
DNA
TPI-GAPDH
Merge
OGC
GIC-1
GIC-2

B

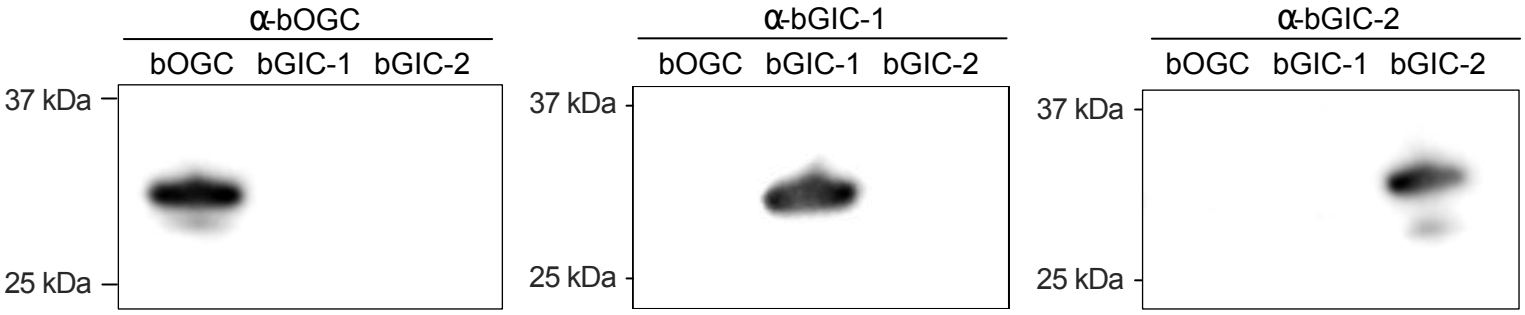
α-bOGC
bOGC bGIC-1 bGIC-2
37 kDa
25 kDa
α-bGIC-1
bOGC bGIC-1 bGIC-2
37 kDa
25 kDa
α-bGIC-2
bOGC bGIC-1 bGIC-2
37 kDa
25 kDa

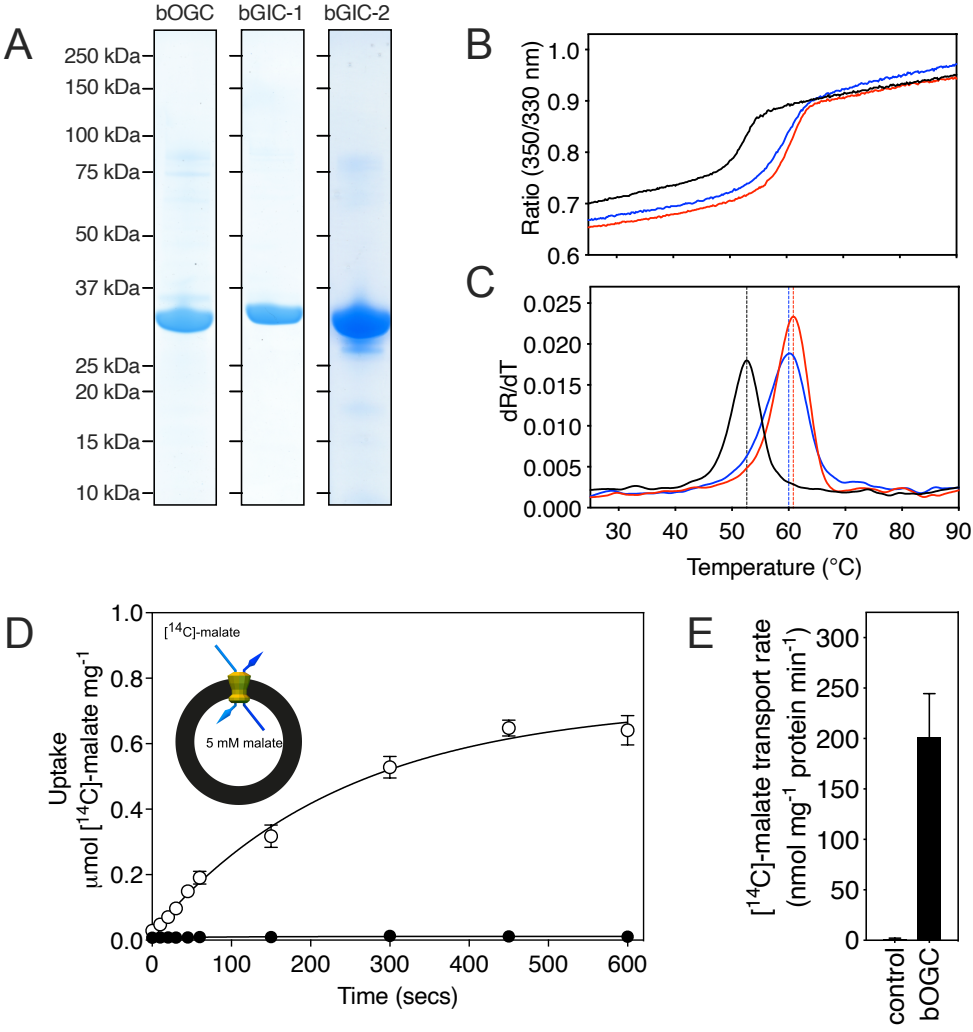
A
bOGC
bGIC-1
bGIC-2
250 kDa
150 kDa
100 kDa
75 kDa
50 kDa
37 kDa
25 kDa
20 kDa
15 kDa
10 kDa
B
Ratio (350/330 nm)
1.0
0.9
0.8
0.7
0.6
C
dR/dT
0.025
0.020
0.015
0.010
0.005
0.000
30
40
50
60
70
80
90
Temperature (°C)
D
[14C]-malate
5 mM malate
Uptake
µmol [14C]-malate mg-1
1.0
0.8
0.6
0.4
0.2
0.0
0
100
200
300
400
500
600
Time (secs)
E
[14C]-malate transport rate
(nmol mg-1 protein min-1)
300
250
200
150
100
50
0
control
bOGC

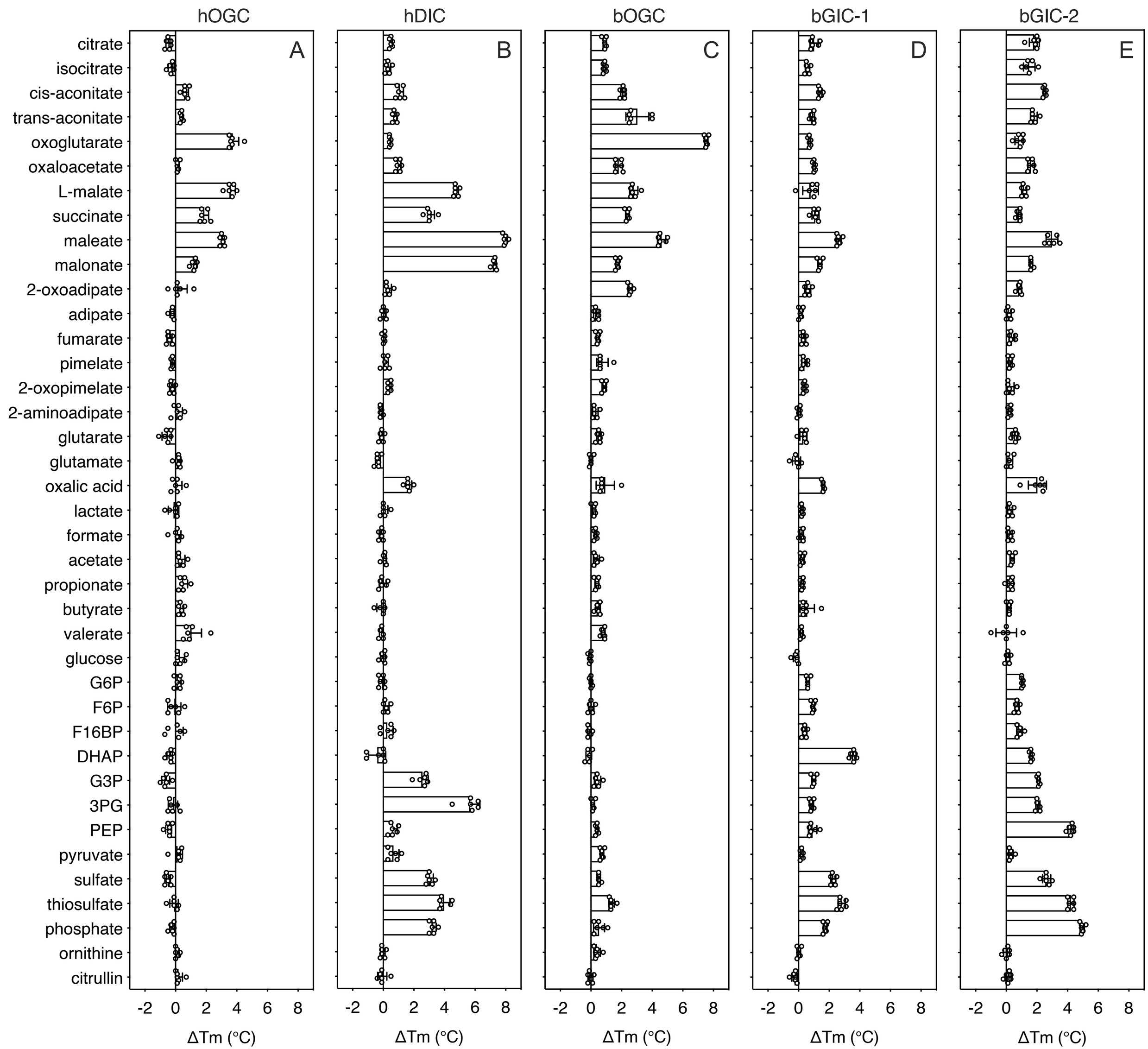
hOGC
hDIC
bOGC
bGIC-1
bGIC-2
A
B
C
D
E
citrate
isocitrate
cis-aconitate
trans-aconitate
oxoglutarate
oxaloacetate
L-malate
succinate
maleate
malonate
2-oxoadipate
adipate
fumarate
pimelate
2-oxopimelate
2-aminoadipate
glutarate
glutamate
oxalic acid
lactate
formate
acetate
propionate
butyrate
valerate
glucose
G6P
F6P
F16BP
DHAP
G3P
3PG
PEP
pyruvate
sulfate
thiosulfate
phosphate
ornithine
citrullin
-2
0
2
4
6
8
ΔTm (°C)

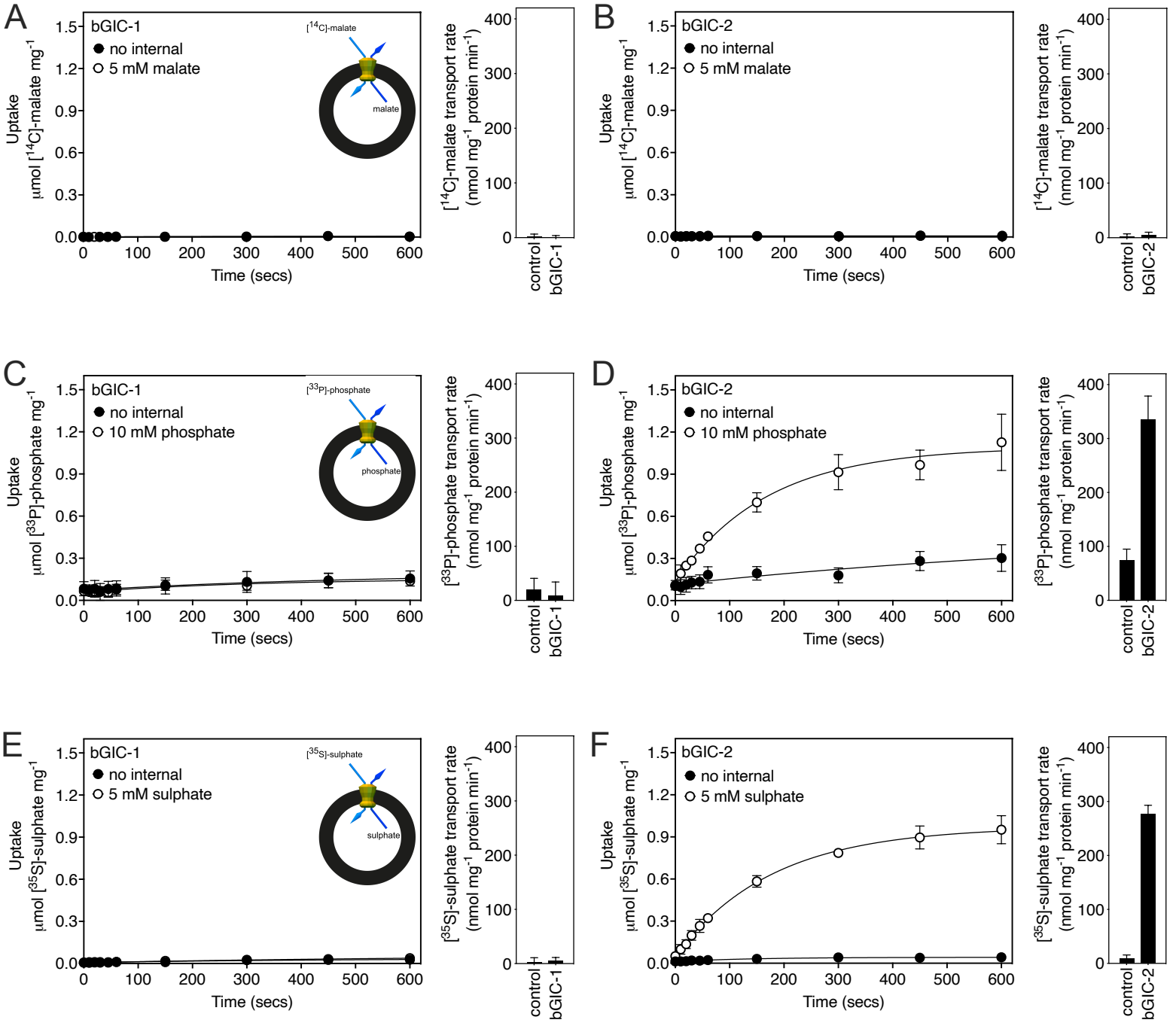
A
bGIC-1
no internal
5 mM malate
[14C]-malate
malate
Uptake
µmol [14C]-malate mg-1
Time (secs)
[14C]-malate transport rate
(nmol mg-1 protein min-1)
control
bGIC-1
B
bGIC-2
no internal
5 mM malate
Uptake
µmol [14C]-malate mg-1
Time (secs)
[14C]-malate transport rate
(nmol mg-1 protein min-1)
control
bGIC-2
C
bGIC-1
no internal
10 mM phosphate
[33P]-phosphate
phosphate
Uptake
µmol [33P]-phosphate mg-1
Time (secs)
[33P]-phosphate transport rate
(nmol mg-1 protein min-1)
control
bGIC-1
D
bGIC-2
no internal
10 mM phosphate
Uptake
µmol [33P]-phosphate mg-1
Time (secs)
[33P]-phosphate transport rate
(nmol mg-1 protein min-1)
control
bGIC-2
E
bGIC-1
no internal
5 mM sulphate
[35S]-sulphate
sulphate
Uptake
µmol [35S]-sulphate mg-1
Time (secs)
[35S]-sulphate transport rate
(nmol mg-1 protein min-1)
control
bGIC-1
F
bGIC-2
no internal
5 mM sulphate
Uptake
µmol [35S]-sulphate mg-1
Time (secs)
[35S]-sulphate transport rate
(nmol mg-1 protein min-1)
control
bGIC-2

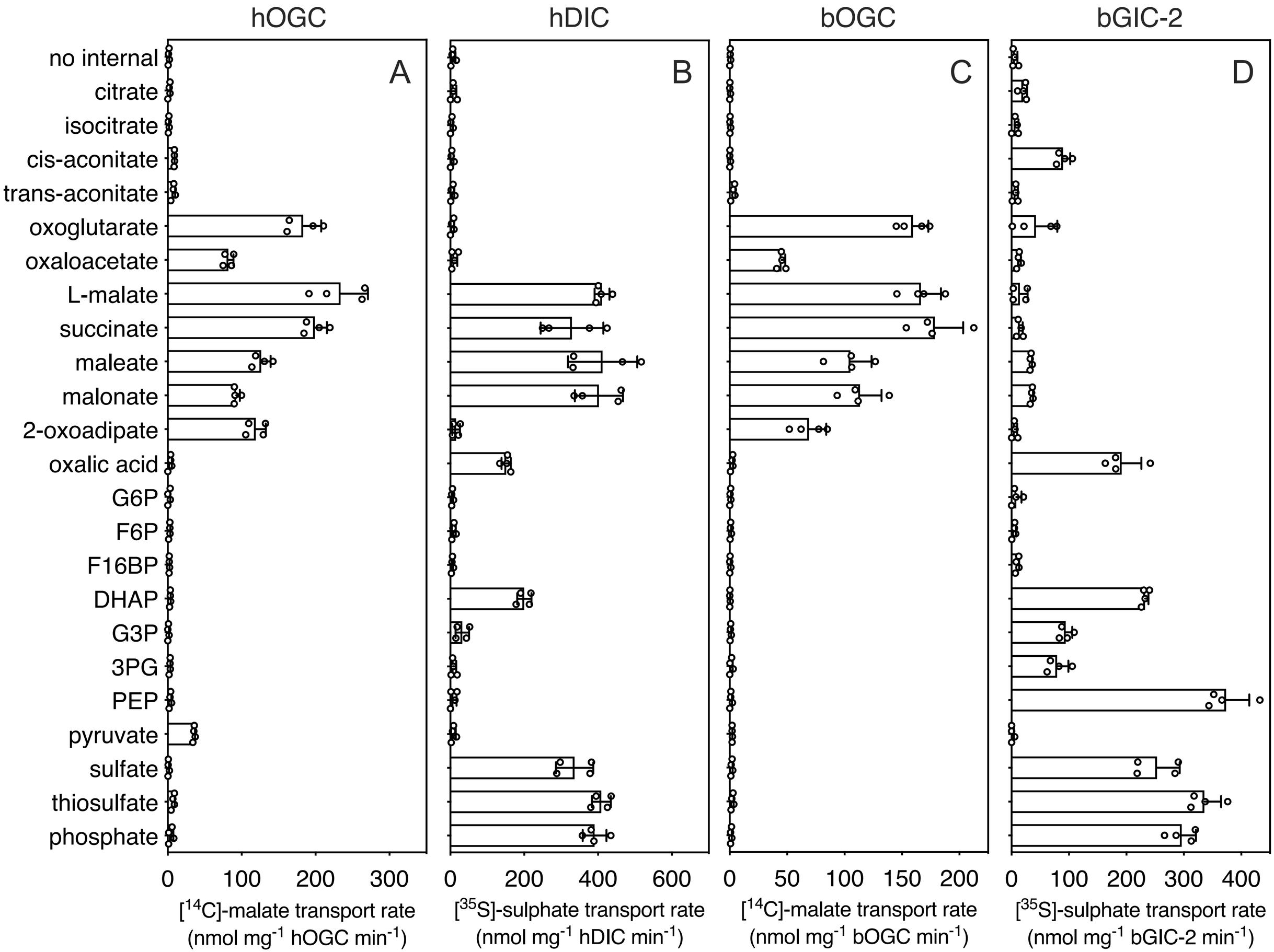
hOGC
hDIC
bOGC
bGIC-2
A
B
C
D
no internal
citrate
isocitrate
cis-aconitate
trans-aconitate
oxoglutarate
oxaloacetate
L-malate
succinate
maleate
malonate
2-oxoadipate
oxalic acid
G6P
F6P
F16BP
DHAP
G3P
3PG
PEP
pyruvate
sulfate
thiosulfate
phosphate
0 100 200 300
[14C]-malate transport rate
(nmol mg-1 hOGC min-1)
0 200 400 600
[35S]-sulphate transport rate
(nmol mg-1 hDIC min-1)
0 50 100 150 200
[14C]-malate transport rate
(nmol mg-1 bOGC min-1)
0 100 200 300 400
[35S]-sulphate transport rate
(nmol mg-1 bGIC-2 min-1)

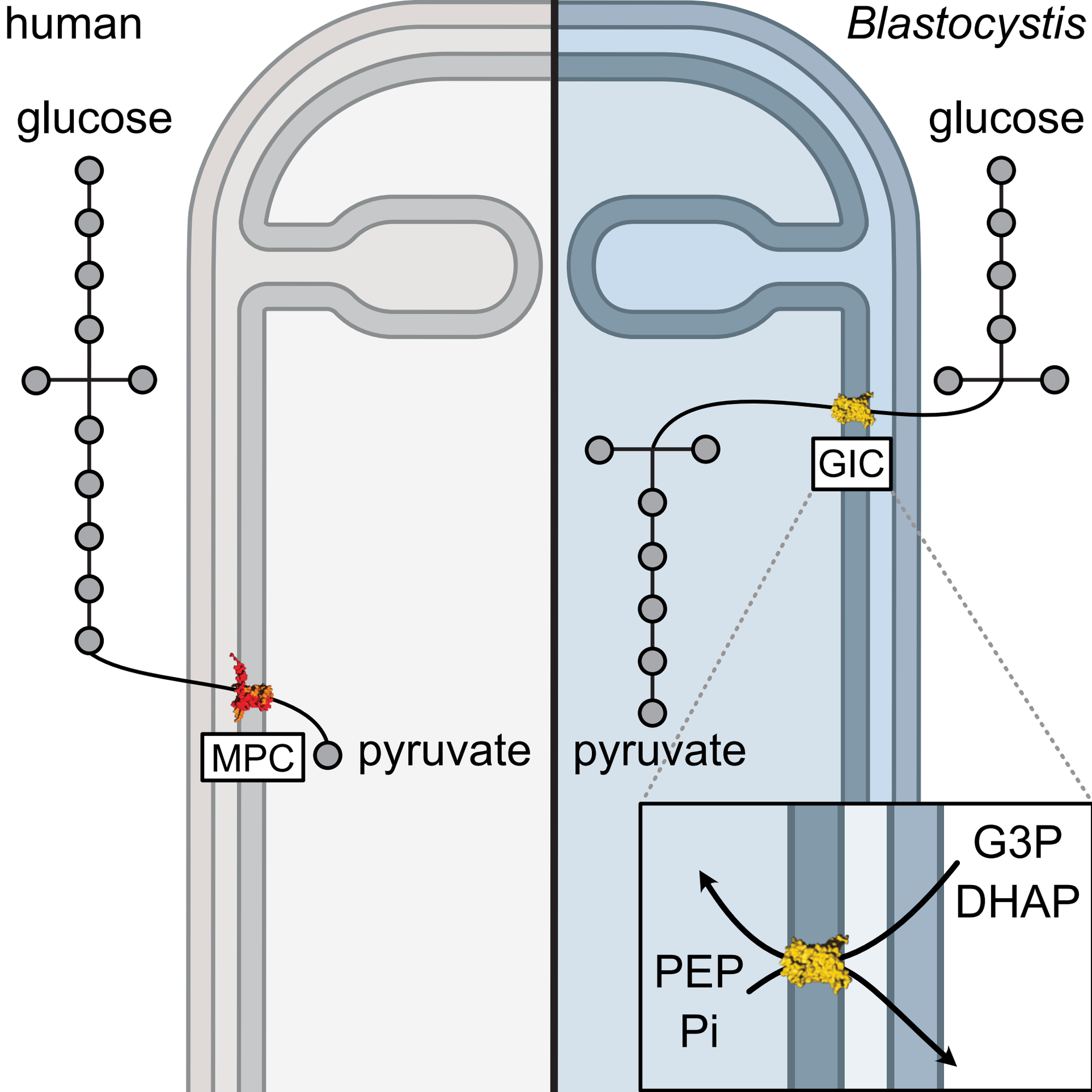
human
glucose
MPC
pyruvate
Blastocystis
glucose
GIC
pyruvate
G3P
DHAP
PEP
Pi